A new computational perceived risk model for automated vehicles based on potential collision avoidance difficulty (PCAD)

He, Xiaolin; Happee, Riender; Wang, Meng

DOI
10.1016/j.trc.2024.104751

Publication date
2024

Document Version
Final published version

Published in
Transportation Research Part C: Emerging Technologies

Citation (APA)
He, X., Happee, R., & Wang, M. (2024). A new computational perceived risk model for automated vehicles based on potential collision avoidance difficulty (PCAD). *Transportation Research Part C: Emerging Technologies*, *166*, Article 104751. https://doi.org/10.1016/j.trc.2024.104751

Transportation Research Part C 166 (2024) 104751

Contents lists available at ScienceDirect

Transportation Research Part C

journal homepage: www.elsevier.com/locate/trc

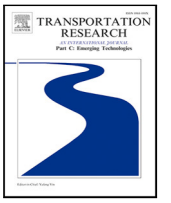

A new computational perceived risk model for automated vehicles based on potential collision avoidance difficulty (PCAD)

Xiaolin He [a,*], Riender Happee [a], Meng Wang [b]

[a] Department of Cognitive Robotics, Delft University of Technology, Mekelweg 2, 2628 CD, Delft, The Netherlands
[b] Chair of Traffic Process Automation,"Friedrich List" Faculty of Transport and Traffic Sciences, Technische Universität Dresden, Hettnerstraße 3, 01069 Dresden, Germany

ARTICLE INFO

Dataset link: https://doi.org/10.4121/3ad2db22-ea82-4436-8df5-ebbbdb4aeec6

Keywords:
Perceived risk
Computational models
Collision avoidance
Task difficulty
Looming

ABSTRACT

Perceived risk is crucial in designing trustworthy and acceptable vehicle automation systems. However, our understanding of perceived risk dynamics remains limited, and corresponding computational models are scarce. This study formulates a new computational perceived risk model based on potential collision avoidance difficulty (PCAD) for drivers of SAE Level 2 automated vehicles. PCAD quantifies task difficulty using the gap between the current velocity and the safe velocity region in 2D, and accounts for the minimal control effort (braking and/or steering) needed to avoid a potential collision, based on visual looming, behavioural uncertainties of neighbouring vehicles, imprecise control of the subject vehicle, and collision severity. The PCAD model predicts both continuous-time perceived risk and peak perceived risk per event. We analyse model properties both theoretically and empirically with two unique datasets: Datasets Merging and Obstacle Avoidance. The PCAD model generally outperforms three state-of-the-art models in terms of model error, detection rate, and the ability to accurately capture the tendencies of human drivers' perceived risk, albeit at the cost of longer computation time. Our findings reveal that perceived risk varies with the position, velocity, and acceleration of the subject and neighbouring vehicles, and is influenced by uncertainties in their velocities.

1. Introduction

Road crashes are a leading cause of injury and death worldwide, resulting in approximately 1.35 million deaths and 20–50 million non-fatal injuries each year (World Health Organization, 2020). Most traffic accidents arise from human misjudgements (Nadimi et al., 2016). Specifically, distorted perception of driving risk by human drivers is one of the important causes of road accidents (Eboli et al., 2017).

Perceived risk captures the level of risk experienced by drivers, which can differ from operational (or actual) risk (Griffin et al., 2020; Kolekar et al., 2020a). A low perceived risk leads to feeling safe, relaxed, and comfortable, while a high-risk perception results in cautious behaviour (Griffin et al., 2020). The advent of active safety and driving automation systems has reduced actual risk, but changes in drivers' risk perception have been observed. Human drivers will inversely perceive a high level of risk if the driving automation shows inappropriate driving behaviours, causing decreased trust, low acceptance, and even refusal of vehicle automation (Xu et al., 2018; Peng et al., 2024). In manual driving, maintaining perceived risk below a specific threshold instigates driver actions, such as steering and braking (Summala, 1988). Consequently, misperception of risk during automated driving may lead to driver distrust, unnecessary interventions, and even failure to recognise dangerous situations that require drivers'

* Corresponding author.
E-mail address: x.he-2@tudelft.nl (X. He).

https://doi.org/10.1016/j.trc.2024.104751
Received 1 June 2023; Received in revised form 26 June 2024; Accepted 2 July 2024
Available online 30 July 2024

List of notations

Categories	Variable*	Description
Kinematic and Geometric Variables	$\boldsymbol{a}_i$	Acceleration of vehicle i
	$d_{s,n}$	Distance between the subject (s) and neighbouring (n) vehicles
	$\dot{d}_{s,n}$	Distance changing rate between the subject (s) and neighbouring (n) vehicles
	$\boldsymbol{p}_i$	Position of vehicle i
	$\boldsymbol{p}_{il}, \boldsymbol{p}_{ir}$	Left and right reference points on vehicle i (in this study at the front for the subject and at the rear for the neighbouring vehicle)
	$\boldsymbol{v}_i$	Velocity of vehicle i
	$\Delta\boldsymbol{v}_{i,a}$	Acceleration-based velocity of vehicle i based on the known acceleration
	$\Delta\boldsymbol{v}_{i,u}$	Uncertain velocity of vehicle i based on manoeuvre uncertainties
	$\boldsymbol{v}'_i$	Perceived velocity of vehicle i taking into account $\boldsymbol{v}_i$, $\Delta\boldsymbol{v}_{i,u}$ and $\Delta\boldsymbol{v}_{i,a}$
	$\theta^{**}_{sj_1,nj_2}$	Bearing between reference points on subject (s) and neighbouring (n) vehicles
	$\dot{\theta}_{sj_1,nj_2}$	Bearing rate between reference points on subject (s) and neighbouring (n) vehicles
	φ	Heading angle
	$\mathbf{X}_i$	State vector of vehicle i
	X, Y	Longitudinal and lateral directions of the coordinate system
	L, W	Length and width of a vehicle
Avoidance Difficulty Computation	$\boldsymbol{V}$	Safe velocity set
	$\boldsymbol{V}'$	Safe velocity set considering uncertainties and known acceleration
	$\boldsymbol{v}_g$	Velocity gap for collision avoidance difficulty derived as distance between $\boldsymbol{v}'_s$ and $\boldsymbol{V}'$
	$\boldsymbol{v}_{s,V}$ $\boldsymbol{v}_{s,V'}$	Subject velocity in the safe velocity set $\boldsymbol{V}$ and $\boldsymbol{V}'$
	r_i	Direction of the uncertain velocity of vehicle i
	$\mathcal{D}$	Probability density function of a truncated Gaussian distribution
	fb, bb, lb, rb	Forward, backward, left and right bounds of the uncertainty velocity in the probability density function of a truncated Gaussian distribution
	$\boldsymbol{N}$	Probability density function of a normal Gaussian distribution
	$\mathcal{N}$	Cumulative distribution function of a normal Gaussian distribution
	l	Length of an uncertain velocity vector
	$\mathcal{P}$	Conditional probability of an uncertain velocity vector
PCAD Model Components	$R_{PCAD}(t)$	Perceived risk function in PCAD model
	$\mathcal{V}_i$	Perceived velocity function for vehicle i
	$\mathcal{A}$	Avoidance difficulty function
	$\mathcal{W}$	Weighting function
PCAD Model Parameters	$\sigma_{i,X}, \sigma_{i,Y}$	Standard deviations for uncertain velocity distributions of vehicle i
	$t_{i,a}$	Anticipated time for acceleration-based velocity of vehicle i
	α	The exponent of the Weighting function.
	β	The mass ratio $\beta = \frac{M_n}{M_s+M_n}$. M_s and M_n represent the mass of the subject (s) and neighbouring (n) vehicles.
	v_{ref}	A reference velocity in the weighting function $\mathcal{W}$, which can be a velocity limit under specific conditions.

* $i \in \{s, n\}$ with s representing the subject vehicle and n representing the neighbouring vehicle.
** j_1, j_2 represent the numbering of different reference points, which can be 1, 2, 3, ...

intervention. Therefore, it is essential to understand and quantify drivers' perceived risk in driving automation and use it to design driving automation with high technical and perceived safety levels.

A few computational models for perceived risk have been developed, and they can be clustered into two categories: empirical models reliant on data, and physical models grounded in first principles. In the first category, Kolekar et al. (2020a) established a driving risk field (DRF) model considering the probability of an event occurring and the event consequence based on drivers' subjective risk ratings and steering responses. Ping et al. (2018) used deep learning methods to model perceived risk in urban scenarios with factors related to the subject vehicle and the driving environment. Our previous study (He et al., 2022) built a regression-based perceived risk model to explain and compute event-based perceived risk in highway merging and braking scenarios. Among other factors, the model captures the influence of relative motion with respect to other road users on drivers' subjective perceived risk ratings.

Physical perceived risk models typically rely on surrogate measures of safety (SMoS). The minimum time to collision (TTC) can show the drivers' threshold of perceived risk when they take last-moment braking actions (Kiefer et al., 2005), while the inverse TTC represents drivers' relative visual expansion of an obstacle, which can indicate drivers' risk perception (Lee, 1976). Additionally, Kondoh et al. (2008, 2014) further analysed the relationship between drivers' risk perception regarding the leading

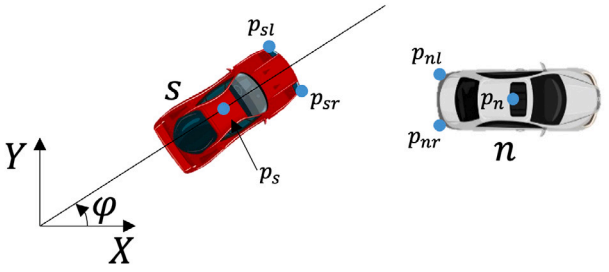

Fig. 1. The coordinate system in the definition.

vehicle and inverse TTC and time headway (THW) in car-following situations. Models using TTC and THW only capture one-dimensional (1D) interaction and are mainly validated for car following. Attempts have been made to model risk for two-dimensional (2D) motion based on the driving risk field theory (Wang et al., 2016) and develop collision warning algorithms (Li et al., 2020). This research line is advanced by the probabilistic driving risk field model (PDRF) (Mullakkal-Babu et al., 2020) by considering motion probability distributions of other road users and the collision severity to estimate the collision risk. Although the above-mentioned models estimate the actual collision risk rather than the perceived risk, they are promising to predict human drivers' risk perception thanks to the strong connection between the actual risk and the perceived risk.

The existing empirical models can quantify perceived risk in certain scenarios, but their validity across diverse situations remains an open question and they are not fully explainable. Physical models, while explainable, can compute the actual risk. However, the mapping between the actual collision risk and perceived risk remains ambiguous and the thresholds of the SMoSs lack empirical support. Hence, an explainable and empirically underpinned computational perceived risk model is still lacking.

This study has two primary objectives: **Objective 1** is to formulate an explainable computational perceived risk model grounded in the human drivers' risk perception mechanism applicable to general 2D movements. **Objective 2** is to analyse and compare our new model with existing models both theoretically and empirically. Our model is defined using the gap between the current velocity and the safe velocity region in 2D. It represents the minimal control effort (braking and/or steering) needed to avoid a potential collision, considering behavioural uncertainties of neighbouring vehicles and imprecise control of the subject vehicle as well as collision severity. Our model predicts both continuous-time perceived risk and peak perceived risk per event. We remark that the proposed model is developed towards the general driver population instead of personalised modelling but can capture individual differences by tuning model parameters.

The remainder of this paper is structured as follows. We first revisit three computational perceived risk models from literature in Section 2, and then present the formulation of the new model in Section 3. Properties of the new model and the three baseline models are presented in Section 4. Perceived risk data, model calibration approach and model performance indices are introduced in Section 5. The model evaluation results are represented in Section 6 followed by a discussion in Section 7, and conclusions in Section 8.

2. Related perceived risk models

This section introduces the preliminaries for perceived risk modelling and three baseline models for comparison and performance evaluation, while referring to Appendix A for details.

2.1. Coordinate system, reference points and vehicle model

All models in this study employ the same coordinate system. The road space is modelled as a flat Euclidean plane. The X-axis aligns with the direction of the road, while the Y-axis is perpendicular to it, oriented counter-clockwise, as illustrated in Fig. 1. Given our focus on perceived risk based on relative motion, rather than vehicle dynamics, we employ a simple point mass model incorporating vehicle dimensions. According to the point mass model, the positions, velocities and accelerations of the geometric centre for both the subject vehicle s and a neighbouring vehicle or obstacle n are $\boldsymbol{p}_s = [x_s, y_s]^T$, $\boldsymbol{p}_n = [x_n, y_n]^T$, $\boldsymbol{v}_s = [v_{s,X}, v_{s,Y}]^T$, $\boldsymbol{v}_n = [v_{n,X}, v_{n,Y}]^T$, $\boldsymbol{a}_s = [a_{s,X}, a_{s,Y}]^T$, $\boldsymbol{a}_n = [a_{n,X}, a_{n,Y}]^T$ respectively. The heading angle φ follows from the vehicle velocity direction for the point mass model.

Vehicle dimensions are incorporated into the perceived risk models. Fig. 1 illustrates that the leftmost and the rightmost points in the front side of the subject vehicle and the rear side of the neighbouring vehicle are the reference points in this case. Given the vehicle's length L and width W, in straight driving, the positions of the reference points are $\boldsymbol{p}_{sl} = \boldsymbol{p}_s + [L/2 \quad W/2]^T$ and $\boldsymbol{p}_{sr} = \boldsymbol{p}_s + [L/2 \quad -W/2]^T$ for the subject vehicle, $\boldsymbol{p}_{nl} = \boldsymbol{p}_s + [-L/2 \quad W/2]^T$ and $\boldsymbol{p}_{nr} = \boldsymbol{p}_s + [-L/2 \quad -W/2]^T$ for the neighbouring vehicle.

Table 1
Introduction of existing perceived risk models.

Model	Regression Perceived Risk Model (RPR) (He et al., 2022)	Perceived Probabilistic Driving Risk Field Model (PPDRF) (Mullakkal-Babu et al., 2020)	Driving Risk Field Model (DRF) (Kolekar et al., 2020a)
Introduction	Event-based model derived from a simulator experiment involving 18 merging and braking event types on a 2-lane highway.	Perceived Probabilistic Driving Risk Field Model accounting for behaviour uncertainties of surrounding vehicles in 2D based on predicted collision probability and collision severity.	Represents human drivers' risk perception as a 2-dimensional field combining probability and consequence of an event.
Assumptions	• Perceived risk stems from vehicles directly in front after entering the lane. • Drivers can accurately estimate motion information.	• Uncertainties of neighbouring vehicles are represented by independent Gaussian distributions of 2D accelerations. • The subject vehicle maintains the current acceleration over the prediction horizon.	• Perceived risk is the product of the probability of a hazardous event and its severity. • The risk field widens with distance and decays with lateral and longitudinal distance. • The height of the perceived risk field decays as the lateral and longitudinal distance from the vehicle increases.
Definitions	The perceived risk is calculated using the longitudinal position of the neighbouring vehicle and the subject vehicle, along with the current acceleration of the neighbouring vehicle. The perceived risk is given as Eq. (A.2).	• Total perceived risk is calculated as a sum of kinetic risk and potential risk as Eq. (A.3). • Kinetic risk is given by Eq. (A.4), involving the subject mass, mass ratio, relative velocity, and estimated collision probability. • Potential risk is modelled as Eq. (A.6), involving the subject mass, relative velocity and the distance to the obstacle.	• The overall perceived risk is quantified as the product of the probability and the severity of events at different positions relative to the vehicle as shown in Eq. (A.7). • The probability field is modelled as a Gaussian distribution in the lateral direction in Eq. (A.8) • The height of the probability field is a function of the longitudinal distance as shown in Eq. (A.9), and the width of the probability field increases linearly with the distance to the obstacle, reflecting widening of the risk field as shown in Eq. (A.10).
Risk diagram	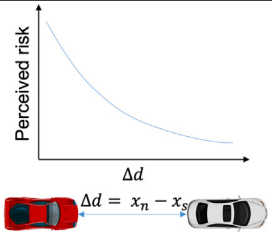	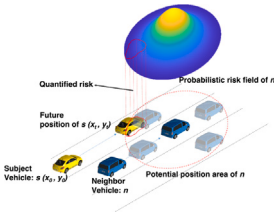	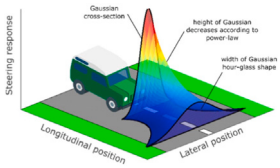

2.2. Existing perceived risk models

In this section, we briefly revisit three perceived risk models that are fundamental to understanding driver's perceived risk in different driving scenarios. These models, including the Regression Perceived Risk Model (RPR) (He et al., 2022), the Perceived Probabilistic Driving Risk Field Model (PPDRF) (Mullakkal-Babu et al., 2020), and the Driving Risk Field Model (DRF) (Kolekar et al., 2020a), offer diverse approaches to quantifying and analysing perceived risk. For a comprehensive overview of these models, including their key assumptions and mathematical definitions, please refer to Table 1 with more details in Appendix A and corresponding literature.

Table 2, summarises model features and factors used in risk calculation. RPR and DRF are validated but do not take into account all factors known to be relevant in risk perception. PPDRF takes into account all listed factors, but its parameters are not based on empirical data and it has not been validated. Hence, this paper presents the new Potential Collision Avoidance Difficulty (PCAD) model which is inspired by the three existing models and validates the resulting four models with the two available perceived risk datasets used to develop and validate the RPR and the DRF model.

3. Potential collision avoidance difficulty model (PCAD)

Our proposed model is grounded in Fuller's Risk Allostasis Theory which proposes that a feeling of risk can be indicated by the driving task difficulty (Fuller, 2011) where drivers' primary driving task is to perform avoidance actions to moderate the perceived risk to a preferred range (Fuller, 1984). Consequently, we develop a dynamic perceived risk model by quantifying the driving task difficulty, which computes real-time perceived risk and explains its underlying mechanism. The PCAD model quantifies the

Table 2
Model features and factors used in risk calculation.

	RPR	PPDRF	DRF	PCAD
Dimension	1-D	2-D	2-D	2-D
Distance	●	●	●	●
Using relative velocity	–	●	–	●
Using acceleration	●	●	–	●
Using subject velocity	–	●	●	●
Considering crash consequence	–	●	●	●
Considering manoeuvre uncertainties	–	●	–	●
Usable on curved lanes	–	●	●	●

● indicate "yes" and – indicate "no".

task difficulty considering the minimal 2D velocity change to avoid a potential collision. The model accounts for the manoeuvre uncertainties of other road users and the imprecision in the control of the subject vehicle.

In this section, we introduce the primary assumptions and the general structure of the model followed by a detailed explanation of each component, including the potential collision judgement method and the perceived velocity of a neighbouring vehicle and the subject vehicle, and a weighting function that considers the collision severity.

3.1. Assumptions

To operationalise the model, we adopt several simplifying assumptions:

- **Assumption 1**: Human drivers perceive risk based on an estimation of the difficulty in avoiding a potential collision according to their visual perception of the relative motion of the subject vehicle and neighbouring vehicles (Fuller, 1984, 2011; Sivak, 1996). They judge whether a vehicle is on a collision course based on looming (Ward et al., 2015).
- **Assumption 2**: The known acceleration and manoeuvre uncertainties of neighbouring and subject vehicles cause extra perceived risk. The latter is presented as an uncertain acceleration following a specific probability distribution. In this study, we assume a Gaussian distribution with zero means. This is grounded in existing literature. In stable highway driving, the longitudinal and lateral accelerations of a neighbour follow a Gaussian distribution (Wagner et al., 2016). Specifically, Ko et al. (2010) observed that in a vehicle field test with GPS, the modelling results of acceleration as a response variable indicated that it followed a Gaussian distribution. Additionally, Jansson (2005) argued that a constant acceleration model is sufficiently accurate for tracking vehicle motion. Both the known acceleration and this uncertain acceleration will remain constant in a short period of time.
  - **2a**: The known accelerations of the subject and neighbouring vehicles influence perceived risk (Herman et al., 1959; Sultan et al., 2004; He et al., 2022).
  - **2b**: The uncertain acceleration of neighbouring vehicles comes from a potential manoeuvre change (e.g., a sudden brake or steer) (Duan et al., 2013; Ding et al., 2014).
  - **2c**: The uncertain acceleration of the subject vehicle is caused by imprecise control in steering and throttle/braking, which is relevant to human drivers' control ability or driving automation's performance (Blaauw, 1982).
- **Assumption 3**: Human drivers perceive higher perceived risk with higher subject vehicle velocity (Kochi et al., 2023).

3.2. General structure of PCAD

Let $\mathbf{X}_s = (\boldsymbol{p}_s, \boldsymbol{v}_s, \boldsymbol{a}_s)^T$ and $\mathbf{X}_n = (\boldsymbol{p}_n, \boldsymbol{v}_n, \boldsymbol{a}_n)^T$ denote the state of the subject vehicle s and the neighbouring vehicle n respectively, with $\boldsymbol{p}_s$ and $\boldsymbol{p}_n$, $\boldsymbol{v}_s$ and $\boldsymbol{v}_n$, $\boldsymbol{a}_s$ and $\boldsymbol{a}_n$ being the position, velocity and acceleration vectors, and T the transpose of a vector. The PCAD is formulated as Eq. (1)

$$R_{PCAD}(t) = \mathcal{A}(\boldsymbol{p}_s, \boldsymbol{p}_n, \mathcal{V}_s(\mathbf{X}_s, \mathbf{X}_n), \mathcal{V}_n(\mathbf{X}_s, \mathbf{X}_n)) \cdot \mathcal{W}(\boldsymbol{v}_s) \tag{1}$$

Here, $\mathcal{A}$ represents the avoidance difficulty function. This function quantifies the required 2D velocity change to bring the subject vehicle to the safe velocity region in the velocity domain to avoid a potential collision with the neighbouring vehicle, considering factors such as their positions, velocities and accelerations. $\mathcal{V}_i$ denotes the 2D perceived velocity for vehicle $i \in \{s, n\}$, thereby capturing absolute and relative motion of the interacting vehicles. Finally, $\mathcal{W}$ is the weighting function, being a power function with v_s, which accounts for the influence of the subject vehicle's speed on perceived risk. Higher speeds generally increase the perceived risk, as the consequence of a potential collision is more severe.

The perceived velocity function $\mathcal{V}_i$ can be represented as

$$\boldsymbol{v}_i' = \mathcal{V}_i(\mathbf{X}_s, \mathbf{X}_n) = \boldsymbol{v}_i + \Delta\boldsymbol{v}_{i,a} + \Delta\boldsymbol{v}_{i,u} \tag{2}$$

where $\mathcal{V}_i$ is the functional operator to compute the perceived velocity $\boldsymbol{v}_i'$ of the vehicle $i \in \{s, n\}$ by human drivers for perceived risk computation. The perceived velocity combines three components: the velocity $\boldsymbol{v}_i$ ($i \in \{s, n\}$), an acceleration-based velocity

$\Delta \boldsymbol{v}_{i,a} (i \in \{s,n\})$ that accounts for the influence of the known acceleration (**Assumption 2a**) and an uncertain velocity $\Delta \boldsymbol{v}_{i,u}$ that accounts for uncertainties in vehicle motion (**Assumption 2b** and **Assumption 2c**). For example, consider a driver who notices that a car ahead is braking rapidly. The driver might perceive the car's velocity to be lower than it actually is because the driver anticipates its future motion based on the acceleration. The uncertain velocity component captures uncertainties in vehicle motion, such as a neighbouring vehicle suddenly swerving or the subject vehicle's imprecise control.

3.3. Collision avoidance difficulty function $\mathcal{A}$ in deterministic conditions

In this section, the collision avoidance difficulty is formulated to capture part of human drivers' perceived risk under constant speed and deterministic motion conditions, and thereby covers **Assumption 1**. The perceived velocity (2) relaxes to the actual velocity $\boldsymbol{v}$ under such conditions. Uncertainties and acceleration will be incorporated in the next section.

3.3.1. Potential collision judgement of human drivers — Looming detection

A precedent step for collision avoidance is to detect a potential collision based on the current environment information. One lesson from aircraft pilots is that two aircraft are on a crossing course if they remain at the same bearing[1] in their field of view. Similarly, in road traffic, a neighbouring vehicle lies on a crossing course with a subject vehicle, if its bearing does not change (Ward et al., 2015; Crashdashes, 2023). Furthermore, if the vehicle is approaching simultaneously, a phenomenon known as *looming* prevails. This situation indicates a risk of collision. This is illustrated in Figs. 2(a) and 2(b) where the bearing θ at which the subject vehicle sees the neighbouring vehicle remains constant. To identify this phenomenon and anticipate a potential collision is referred to as *looming detection*.

Our method of looming detection combines the two criteria introduced above, requiring that: **(i)** the bearing θ of a neighbouring vehicle remains constant (see Fig. 2(b)), and **(ii)** the distance between the two vehicles is decreasing. Fig. 2(b) illustrates the bearing θ considering each vehicle as a single point, but to detect looming we must also consider vehicle size. Here we approximate vehicle shape by rectangles and use corners as reference points. In the side impact example in Fig. 2(c) the relevant reference points are the front left and front right of the subject vehicle and the front left and rear left of the neighbouring vehicle. We consider four interactions for looming detection. Fig. 2(c) illustrates the four relevant interactions between corners $\boldsymbol{p}_{sl}/\boldsymbol{p}_{nl}$, $\boldsymbol{p}_{sl}/\boldsymbol{p}_{nr}$, $\boldsymbol{p}_{sr}/\boldsymbol{p}_{nl}$, and $\boldsymbol{p}_{sr}/\boldsymbol{p}_{nr}$ respectively. From the perspective of the subject vehicle, the left reference point on the neighbouring vehicle moves to the left (anticlockwise), but the right one moves to the right (clockwise). At an intermediate point the heading rate will be zero, representing a collision. Meanwhile, the distance between the two vehicles is decreasing and hence this is a looming case. Alternatively if both points would move to the left the subject vehicle would pass at the right, and if both points would move to the right the subject vehicle would pass at the left.

In this study, the reference points are chosen at the front left and right on the subject vehicle and the rear left and right on the neighbouring vehicle (Figs. 1 and 3). This simplification is justified since the datasets used contain only obstacle avoidance events and merging events in the front of the subject vehicle.

In our method, the relative bearing rate $\dot{\boldsymbol{\theta}}_{sj_1,nj_2}$ of four pairs of reference points on the subject vehicle and the neighbouring vehicle is calculated using Eq. (3)[2] (see Fig. 2(c) for more details).

$$\dot{\boldsymbol{\theta}}_{sj_1,nj_2} = \frac{\left(\boldsymbol{p}_{sj_1} - \boldsymbol{p}_{nj_2}\right) \times \left(\boldsymbol{v}_{sj_1} - \boldsymbol{v}_{nj_2}\right)}{\left\|\boldsymbol{p}_{sj_1} - \boldsymbol{p}_{nj_2}\right\|^2}, \quad j_1, j_2 \in \{l, r\} \tag{3}$$

Looming is indicated when the product of the minimum and maximum values of $\dot{\boldsymbol{\theta}}_{sj_1,nj_2}$ is negative (one is positive and one is negative), as shown in Eq. (4) and Fig. 2(c).

$$\min \dot{\boldsymbol{\theta}}_{sj_1,nj_2} \cdot \max \dot{\boldsymbol{\theta}}_{sj_1,nj_2} < 0, \quad j_1, j_2 \in \{l, r\}, \tag{4}$$

The second criterion for *looming* is that the neighbouring vehicle is approaching the subject vehicle. That is, a neighbouring vehicle may only collide with the subject vehicle if it is getting closer. This is assessed by examining the distance changing rate between the two vehicles (centre), defined by Eq. (5) and its derivative in Eq. (6). A negative rate indicates that the neighbouring vehicle is approaching.

$$d_{s,n} = \sqrt{(\boldsymbol{p}_s - \boldsymbol{p}_n)^T (\boldsymbol{p}_s - \boldsymbol{p}_n)} \tag{5}$$

$$\dot{d}_{s,n} = \frac{1}{d_{s,n}} (\boldsymbol{p}_s - \boldsymbol{p}_n)^T (\boldsymbol{v}_s - \boldsymbol{v}_n) < 0 \tag{6}$$

Considering the two criteria, if Eqs. (4) and (6) are satisfied at the same time, the neighbouring vehicle is looming (Fig. 2). Conversely, if Eqs. (4) and (6) are not met simultaneously, the neighbouring vehicle is classified as non-looming (Fig. 3), namely

$$\min \dot{\boldsymbol{\theta}}_{sj_1,nj_2} \cdot \max \dot{\boldsymbol{\theta}}_{sj_1,nj_2} \geqslant 0, \quad j_1, j_2 \in \{l, r\}, \tag{7}$$

[1] We define bearing as the orientation in our field of view at which another object is observed.

[2] In straight driving, the velocity of reference points $\boldsymbol{v}_{i,j}$ $(i \in \{s,n\}, j \in \{l,r\})$ can be simplified as the vehicle's linear velocity $\boldsymbol{v}_i$ $(i \in \{s,n\})$ without considering vehicle's yaw rate.

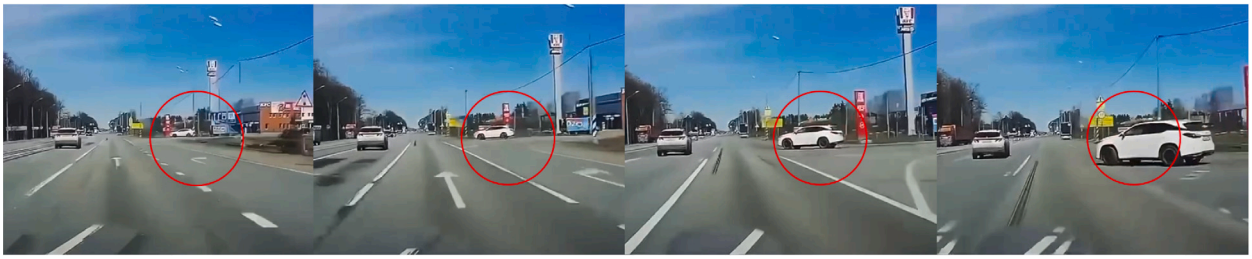

(a) Video stream for a potential collision. The neighbouring vehicle (white) stays at the same bearing (the red circle) and becomes larger when on a crossing course with the subject vehicle (Crashdashes, 2023). Here the bearing is the orientation in the field of view in which another object is observed.

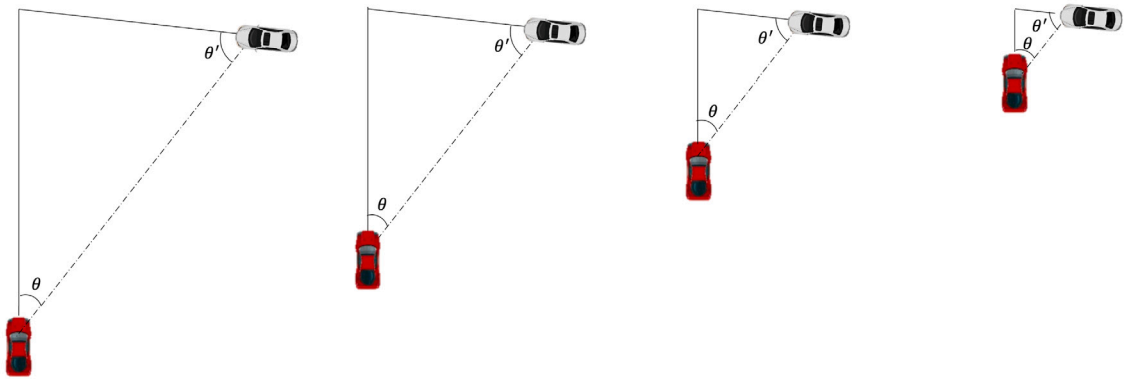

(b) Bird eye view for the potential collision above. The bearings θ and θ' of subject vehicle (red) and neighbouring vehicle (white) remain the same when they are on a crossing course.

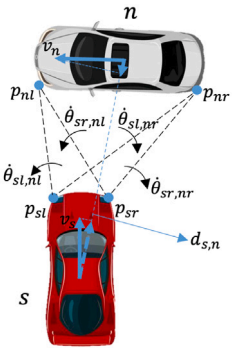

(c) Details for the potential collision above. From the perspective of the subject vehicle, the left reference point on the neighbouring vehicle moves to the left (anticlockwise), but the right one moves to the right (clockwise). Meanwhile, the distance between the two vehicles is decreasing. This case meets looming criteria.

Fig. 2. An example of looming. The subject vehicle and a neighbouring vehicle are on a crossing course.

or

$$\dot{d}_{s,n} = \frac{1}{d_{s,n}}(\boldsymbol{p}_s - \boldsymbol{p}_n)^T(\boldsymbol{v}_s - \boldsymbol{v}_n) \geqslant 0, \tag{8}$$

Note that we examine four pairs of reference points in Eq. (3) and Eq. (4) for a simpler computation. In general circumstances, reference points for collision detection are ideally positioned at the four corner points of each vehicle. If the computation capability permits, we can examine all 16 pairs of reference points for Eq. (3) and Eq. (4). Additionally, *Looming detection* is directly valid when the subject vehicle only has translational motion with constant acceleration and thereby follows a straight path. When the subject vehicle has a yaw rate ($\dot{\varphi}$), and follows a curved path the theory still stands based on a conformal mapping.

3.3.2. Collision avoidance difficulty

We define a safe velocity set $\boldsymbol{V}$, which comprises all non-looming subject velocity vectors that meet Eq. (7) and/or (8) based on the position of the two vehicles $\boldsymbol{p}_s$, $\boldsymbol{p}_s$ and the velocity of the neighbouring vehicle $\boldsymbol{v}_n$ at the current moment. The safe velocity set

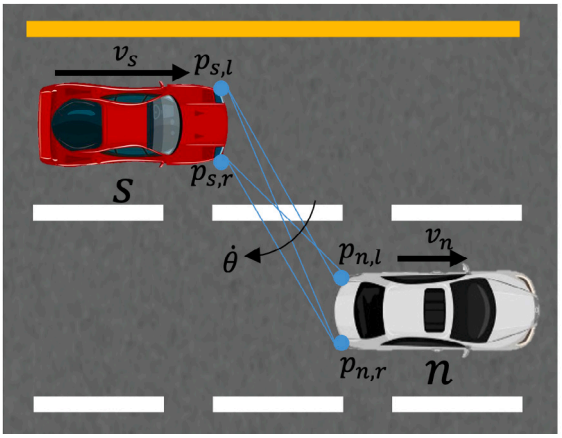

(a) The subject vehicle (Red) is overtaking a neighbouring vehicle (white). Although the neighbour vehicle (White) approaches the subject vehicle (red), the orientation of it in the subject vehicle's view field is not staying constant (all bearing rate regarding all pairs of reference points $\dot{\theta}$ is negative, meaning that the neighbouring vehicle is rotating around the subject vehicle (clockwise)). The situation meets Eq. (6) but does not meet Eq. (4), indicating that it is a non-looming case.

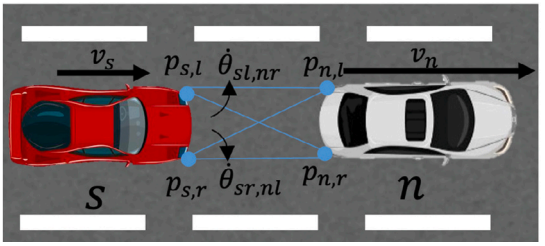

(b) The subject vehicle (red) is following a leading vehicle (white) with a lower speed. Although the orientation of the neighbouring vehicle stays the same in the subject vehicle's view field ($\dot{\theta}_{sl,nr}$ is positive but $\dot{\theta}_{sr,nl}$ is negative), it is not approaching the subject vehicle. The situation meets Eq. (4) but does not meet Eq. (6), indicating that it is a non-looming case.

Fig. 3. Two examples of non-looming.

$\boldsymbol{V}$ is defined in Eq. (9).

$$\forall \boldsymbol{v}_s \in \boldsymbol{V} \Rightarrow \min \dot{\boldsymbol{\theta}}_{sj_1,nj_2} \cdot \max \dot{\boldsymbol{\theta}}_{sj_1,nj_2} \geqslant 0 \ (j_1, j_2 \in \{l, r\},) \text{ or } \dot{d}_{s,n} \geqslant 0, \tag{9}$$

where the equality holds when $\boldsymbol{v}_s$ is at the boundary of velocity set $\boldsymbol{V}$.

The collision avoidance difficulty $\|\boldsymbol{v}_g\|$ is defined as the 2D distance from the current subject velocity $\boldsymbol{v}_s$ to the nearest point on the boundary of the safe velocity set $\boldsymbol{V}$, which is the end point of the vector denoted as $\boldsymbol{v}_{s,V}$ (Eq. (10)) (see Fig. 4 for an illustration). Hence, the collision avoidance function $\mathcal{A}$ is defined as

$$\|\boldsymbol{v}_g\| = \mathcal{A} = \|\boldsymbol{v}_{s,V} - \boldsymbol{v}_s\| \tag{10}$$

where $\boldsymbol{v}_{s,V}$ is the vector in the safe velocity set $\boldsymbol{V}$, the end point of which is closest to the subject velocity vector $\boldsymbol{v}_s$, satisfying

$$\boldsymbol{v}_{s,V} = \arg\min_{\boldsymbol{v} \in \boldsymbol{V}} \|\boldsymbol{v} - \boldsymbol{v}_s\| \tag{11}$$

$\boldsymbol{v}_g$ represents the vector pointing from the current subject velocity $\boldsymbol{v}_s$ towards $\boldsymbol{v}_{s,V}$, indicating the direction and magnitude of the adjustment needed to reach the safe velocity set $\boldsymbol{V}$ from the current velocity $\boldsymbol{v}_s$. If the current subject velocity $\boldsymbol{v}_s$ already lies within the safe velocity set $\boldsymbol{V}$, then the velocity gap $\|\boldsymbol{v}_g\|$ is zero, implying no collision avoidance difficulty.

In this study, the technique of grid search is employed to identify $\boldsymbol{v}_g$, ensuring compliance with both Eq. (10) and Eq. (11).

3.4. Perceived velocity function $\mathcal{V}_i$ of a neighbouring vehicle and the subject vehicle considering known acceleration and manoeuvre uncertainties

The collision avoidance difficulty calculated using the actual (deterministic) motion information (i.e., $\boldsymbol{p}_i$ and $\boldsymbol{v}_i$) (Eq. (10)) presented in the previous section can already account for most of the perceived risk, which is shown in Section 6 (Figs. 10(e) and 11(e)). However, these calculations overlook how human drivers process environmental information considering known accelerations and uncertainties. In this section, we define a perceived velocity function denoted as $\mathcal{V}$ shown in Eq. (2) for both the subject and the neighbouring vehicles. This function is based on a more comprehensive understanding, which outputs a perceived velocity $\boldsymbol{v}_i'$ consisting of three components: the actual velocity $\boldsymbol{v}_i$, the velocity derived from the known acceleration $\boldsymbol{v}_{i,a}$ and the velocity derived from manoeuvre uncertainties $\boldsymbol{v}_{i,u}$. The perceived velocity yields an adjusted safe velocity set $\boldsymbol{V}'$ and thereby a new velocity gap $\boldsymbol{v}_g$.

3.4.1. The perceived velocity

The perceived velocity $\boldsymbol{v}_i'$ is the final output of perceived velocity function $\mathcal{V}$ based on the state of the subject vehicle $\mathbf{X}_s = (\boldsymbol{p}_s, \boldsymbol{v}_s, \boldsymbol{a}_s)^T$ and the state of the neighbouring vehicle $\mathbf{X}_n = (\boldsymbol{p}_n, \boldsymbol{v}_n, \boldsymbol{a}_n)^T$, which consists of the actual velocity $\boldsymbol{v}_i$, the known acceleration-based velocity $\Delta\boldsymbol{v}_{i,a}$ and the uncertain velocity $\Delta\boldsymbol{v}_{i,u}$ as shown in Eq. (2). This integrated perceived velocity function considers the acceleration and uncertainties, thus contributing to extra perceived risk. Fig. 5 illustrates the relationship between the

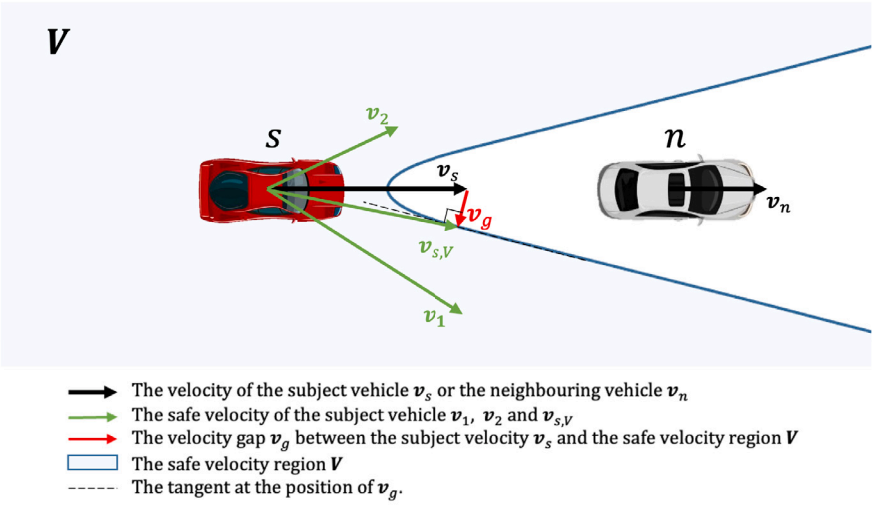

Fig. 4. An example to show the collision avoidance difficulty. In this case, the subject vehicle (red) is following a leading vehicle (white, 50 m ahead, $v_n = 8.33$ m/s) with a higher velocity ($v_s = 16.67$ m/s). Eq. (7) and (8) define the safe velocity set V as the blue area, e.g., if the current subject velocity is any one of the elements in V (e.g., v_1 and v_2), the neighbouring vehicle (white) is not looming, and the collision avoidance difficulty is zero. In this example, since the subject vehicle is driving faster than the leading vehicle, the current subject velocity $v_s \notin V$, indicating that the neighbouring is looming regarding the subject vehicle. The distance from the subject velocity v_s to the safe velocity set V (the safety boundary) is v_g (the red arrow), the length of which is the defined collision avoidance difficulty.

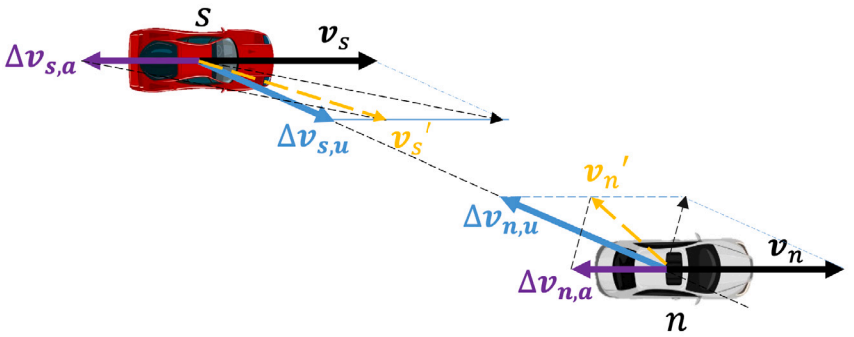

Fig. 5. The relationship between the actual velocity v_i the uncertain velocity $\Delta v_{i,u}$, the acceleration caused velocity change and the perceived velocity v_i' ($i \in \{s, n\}$) of the subject vehicle s and the neighbouring vehicle n. In this case, the subject vehicle (red) is passing by a neighbouring vehicle (white). Both vehicles are decelerating causing acceleration-based velocities $\Delta v_{s,a}$ and $\Delta v_{n,a}$ (the purple arrows). The uncertain velocities $\Delta v_{s,u}$ and $\Delta v_{n,u}$ are pointing to each other. The final perceived velocity v_s' and v_n' contain the contribution of the acceleration-based velocity and the uncertain velocity.

actual velocity v_i, the uncertain velocity $\Delta v_{i,u}$, the acceleration-based velocity $\Delta v_{i,a}$ and the final perceived velocity v_i'. The perceived velocity v_i' is utilised for computing perceived risk. The known acceleration-based velocity $\Delta v_{i,a}$ and the uncertain velocity $\Delta v_{i,u}$ will be detailed in Sections 3.4.2 and 3.4.3 below.

3.4.2. The velocity component derived from known acceleration — the acceleration-based velocity

Previous studies have shown that human drivers consider the acceleration of the subject and other vehicles during driving (Herman et al., 1959). A collision avoidance behaviour model for drivers achieves 20% more accuracy when the acceleration of other vehicles is considered (Sultan et al., 2004). For example, the action of braking by a leading vehicle can initially cause perceived risk to the following subject vehicle, even if the distance between the vehicles does not close rapidly at the initial stage. The perceived risk may decrease once the subject vehicle also brakes, even as the gap between the vehicles continues to decrease.

To account for the influence of known acceleration (**Assumption 2a**), we introduce a component to the perceived velocity (Eq. (2), which reflects human drivers' anticipation of velocity based on the current known acceleration. We name this component as acceleration-based velocity represented by Eq. (12).

$$\Delta v_{i,a} = a_i \cdot t_{i,a}, \quad i \in \{s, n\} \tag{12}$$

where $\Delta \boldsymbol{v}_{i,a}$ represents the component of perceived velocity caused by known acceleration; $\boldsymbol{a}_i$ is the current acceleration, and $t_{i,a}$ is an anticipated time for computation that varies for the subject vehicle and the neighbouring vehicle. $t_{i,a}$ is determined by calibration. The impact of $t_{i,a}$ duration on the model behaviour depends on the known acceleration direction. If the known acceleration tends to decrease the gap between two vehicles, a longer anticipated time results in a higher perceived risk output by the model, and vice versa.

3.4.3. The velocity component derived from manoeuvre uncertainties — the uncertain velocity

Assumption 2b and **Assumption 2c** specify that manoeuvre uncertainties cause additional perceived risk. For instance, when we pass by a car in the adjacent lane, we unconsciously shift to the other side of the lane to keep away from the car for safety because the velocity of the other car can suddenly change (Ding et al., 2014). Accordingly, we define an uncertain velocity perceived by human drivers based on the manoeuvre uncertainties as a component of the perceived velocity (Eq. (2)).

The uncertain velocity in human driver's mind caused by the uncertainties of each vehicle in interaction makes the situation being perceived as more dangerous. Fig. 6 shows an example of the uncertain velocity and its influence on the velocity set $\boldsymbol{V}$.

The uncertain velocity exists in all directions on both subject and neighbouring vehicles, but its impact for different directions on perceived risk varies. We assume that acceleration with a direction reducing the distance between vehicles most strongly increases perceived risk. Hence we only consider this direction in the perceived risk model, which also reduces computational complexity. This direction is illustrated in Fig. 5, with a detailed explanation in Appendix D.

Based on the discussion above, we have

$$\Delta \boldsymbol{v}_{i,u} = l \cdot \frac{\boldsymbol{p}_s - \boldsymbol{p}_n}{\|\boldsymbol{p}_s - \boldsymbol{p}_n\|} \cdot r_i, \quad i \in \{s, n\}, \quad r_n = 1 \quad \text{and} \quad r_s = -1. \tag{13}$$

where $\Delta \boldsymbol{v}_{i,u}$ ($i \in \{s, n\}$) is the uncertain velocity; l is the length of the uncertain velocity vector which is derived below; $\frac{\boldsymbol{p}_s - \boldsymbol{p}_n}{\|\boldsymbol{p}_s - \boldsymbol{p}_n\|}$ is a unit vector pointing from the neighbouring vehicle to the subject vehicle; r determines the direction of the uncertain velocity where $r_n = 1$ is for the neighbouring vehicle representing the direction from the neighbouring vehicle to the subject vehicle, and $r_s = -1$ is for the subject vehicle representing the opposite direction.

According to **Assumption 2b** and **2c**, the manoeuvre uncertainties are presented as an uncertain acceleration, which is assumed to follow Gaussian distributions as motivated under Assumption 2, and this acceleration will remain constant over a short period of time. Hence, given a specific duration, the uncertain velocity $\Delta \boldsymbol{v}_{i,u}$ ($i \in \{s, n\}$) also follows Gaussian distributions. With the consideration of physical restrictions of the vehicle velocity, the Gaussian is

$$\begin{aligned} v_{i,u,X} &\sim \mathcal{D}(v_{i,u,X} | 0, \sigma_{i,X}, fb, bb) \\ v_{i,u,Y} &\sim \mathcal{D}(v_{i,u,Y} | 0, \sigma_{i,Y}, lb, rb) \end{aligned} \tag{14}$$

where $v_{i,u,X}$ and $v_{i,u,Y}$ are the uncertain velocity in X and Y directions; D is the probability density function of the uncertain velocity in each direction. fb, bb, lb, rb are the forward, backward, left and right bounds for the uncertain velocity in the density function, which are set to 50 m/s, −14 m/s, 8.5 m/s and −8.5 m/s respectively in this study (Jazar, 2008). The truncated distribution D becomes

$$\begin{aligned} \mathcal{D}(v_{i,u,X} | 0, \sigma_{i,X}, fb, bb) &= \begin{cases} \dfrac{\frac{1}{\sigma_{i,X}} N(\frac{v_{i,u,X}}{\sigma_{i,X}})}{\mathcal{N}(\frac{fb - v_{i,X}}{\sigma_{i,X}}) - \mathcal{N}(\frac{bb - v_{i,X}}{\sigma_{i,X}})}, & bb \leqslant v_{i,u,X} \leqslant fb, i \in \{s, n\} \\ 0, \quad \text{otherwise} \end{cases} \\ \mathcal{D}(v_{i,u,Y} | 0, \sigma_Y, lb, rb) &= \begin{cases} \dfrac{\frac{1}{\sigma_{i,Y}} N(\frac{v_{i,u,Y}}{\sigma_{i,Y}})}{\mathcal{N}(\frac{lb - v_{i,Y}}{\sigma_{i,Y}}) - \mathcal{N}(\frac{rb - v_{i,Y}}{\sigma_{i,Y}})}, & rb \leqslant v_{i,u,Y} \leqslant lb, i \in \{s, n\} \\ 0, \quad \text{otherwise} \end{cases} \end{aligned} \tag{15}$$

where N is the probability density function of the Gaussian distribution and $\mathcal{N}$ is its cumulative distribution function.

To obtain the final uncertain velocity, its length and direction should be considered simultaneously. Hence, we use the mathematical expectation of Eq. (13) as the length of the uncertain velocity, which can be calculated as follows

$$\begin{aligned} E(\|\Delta \boldsymbol{v}_{i,u}\|) &= \int_0^{+\infty} \mathcal{P}\left(\Delta \boldsymbol{v}_{i,u} \middle| \frac{\boldsymbol{p}_s - \boldsymbol{p}_n}{\|\boldsymbol{p}_s - \boldsymbol{p}_n\|}, l \right) \cdot l \, dl \\ &= \int_0^{+\infty} \mathcal{D}(v_{i,u,X} | 0, \sigma_{i,X}, fb, bb) \cdot \mathcal{D}(v_{i,u,Y} | 0, \sigma_{i,Y}, lb, rb) \cdot \frac{1}{\mathcal{P}\left(\frac{\boldsymbol{p}_s - \boldsymbol{p}_n}{\|\boldsymbol{p}_s - \boldsymbol{p}_n\|} \right)} \cdot l \, dl \end{aligned} \tag{16}$$

This conditional probability is denoted by $\mathcal{P}\left(\Delta \boldsymbol{v}_{i,u} \middle| \frac{\boldsymbol{p}_s - \boldsymbol{p}_n}{\|\boldsymbol{p}_s - \boldsymbol{p}_n\|}, l \right)$, representing that an uncertain velocity $\boldsymbol{v}_{i,u}$ with length l is on the line connecting the subject vehicle and the neighbouring vehicle. To ensure that this direction-specific probability is considered, we divide the product of the two probability density functions, $\mathcal{D}(v_{i,u,X} | 0, \sigma_{i,X}, fb, bb)$ and $\mathcal{D}(v_{i,u,Y} | 0, \sigma_{i,Y}, lb, rb)$, by the aforementioned conditional probability $\mathcal{P}\left(\frac{\boldsymbol{p}_s - \boldsymbol{p}_n}{\|\boldsymbol{p}_s - \boldsymbol{p}_g\|} \right)$. This division effectively normalises the probability densities and allows for the proper calculation of the mathematical expectation of the length of the uncertain velocity $E(\|\Delta \boldsymbol{v}_{i,u}\|)$.

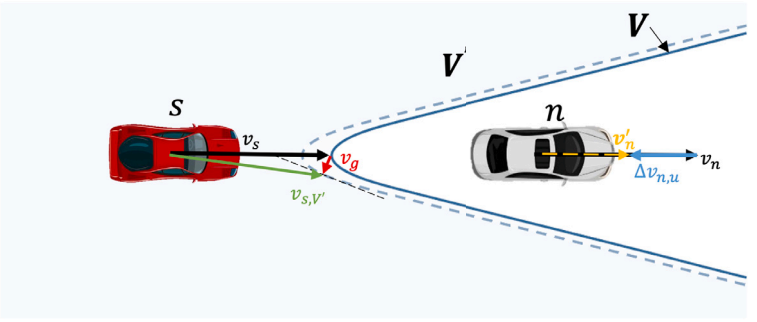

(a) The uncertain velocity $\Delta \boldsymbol{v}_{n,u}$, the final perceived velocity of the neighbouring vehicle $\boldsymbol{v}'_n$ and their influence on safe velocity set $\boldsymbol{V}$. Note that $\Delta \boldsymbol{v}_{s,a}$, $\Delta \boldsymbol{v}_{s,u}$ and $\Delta \boldsymbol{v}_{n,a}$ are not taken into account to show only the influence of the uncertain velocity $\Delta \boldsymbol{v}_{n,u}$ on the safe velocity set $\boldsymbol{V}$ and finally the velocity gap $\boldsymbol{v}_g$ for collision avoidance difficulty. $\boldsymbol{v}_s \in \boldsymbol{V}$ indicates collision avoidance difficulty is originally zero. However, the human driver inside the subject vehicle perceives an uncertain velocity $\Delta \boldsymbol{v}_{n,u}$ (the blue arrow on the neighbouring vehicle) of the leading vehicle considering the uncertainties, changing the neighbouring vehicle's velocity from $\boldsymbol{v}_n$ to $\boldsymbol{v}'_n$ (the yellow dashed arrow on the neighbouring vehicle, which is the perceived velocity of the neighbouring vehicle). Correspondingly, the velocity set $\boldsymbol{V}$ becomes $\boldsymbol{V}'$ that is smaller than $\boldsymbol{V}$ based on the perceived velocity $\boldsymbol{v}'_n$, which leads to $\boldsymbol{v}_s \notin \boldsymbol{V}'$ causing extra perceived risk.

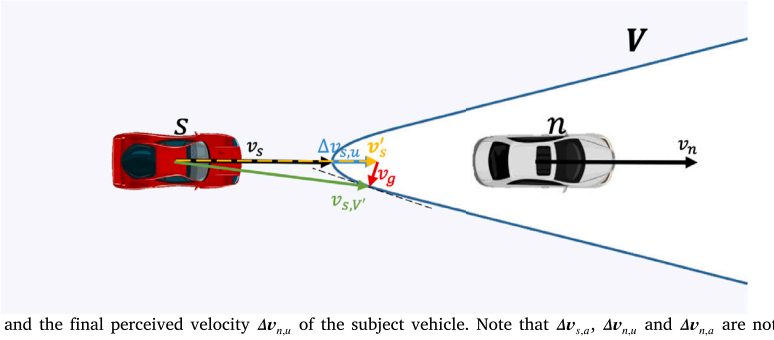

(b) The uncertain velocity $\Delta \boldsymbol{v}_{s,u}$ and the final perceived velocity $\Delta \boldsymbol{v}_{n,u}$ of the subject vehicle. Note that $\Delta \boldsymbol{v}_{s,a}$, $\Delta \boldsymbol{v}_{n,u}$ and $\Delta \boldsymbol{v}_{n,a}$ are not taken into account to show only the influence of the uncertain velocity $\Delta \boldsymbol{v}_{s,u}$ on the velocity gap $\boldsymbol{v}_g$ for collision avoidance difficulty. $\boldsymbol{v}_s \in \boldsymbol{V}$ indicates collision avoidance difficulty is originally zero. However, the human driver inside the subject vehicle perceives an uncertain velocity $\Delta \boldsymbol{v}_{s,u}$ (the blue arrow on the subject vehicle) due to human drivers' inaccurate control or imperfect control of driving automation, making the subject velocity change from $\boldsymbol{v}_s$ to $\boldsymbol{v}'_s$ (the yellow dashed arrow on the subject vehicle, which is the perceived velocity of the subject vehicle). The perceived velocity $\boldsymbol{v}'_s \notin \boldsymbol{V}$, causing extra perceived risk.

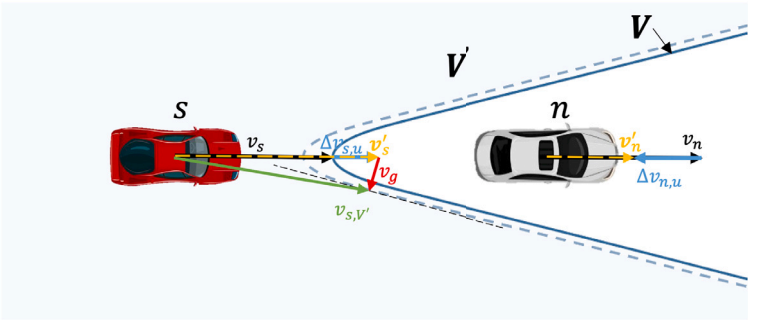

(c) The perceived velocity set $\boldsymbol{V}'$ based on the perceived velocity. Note that $\Delta \boldsymbol{v}_{s,a}$ and $\Delta \boldsymbol{v}_{n,a}$ are not taken into account to show only the combined influence of uncertain velocities $\Delta \boldsymbol{v}_{s,u}$ and $\Delta \boldsymbol{v}_{n,u}$ on the safe velocity $\boldsymbol{V}$ and the velocity gap $\boldsymbol{v}_g$ for collision avoidance difficulty. With the larger perceived subject velocity $\boldsymbol{v}'_s$ and the smaller perceived velocity set $\boldsymbol{V}'$ simultaneously, $\boldsymbol{v}'_s \notin \boldsymbol{V}'$. $\boldsymbol{v}_g$ is the distance from the perceived subject velocity to the boundary of the perceived safe velocity set $\boldsymbol{V}'$, which is the perceived risk in this study.

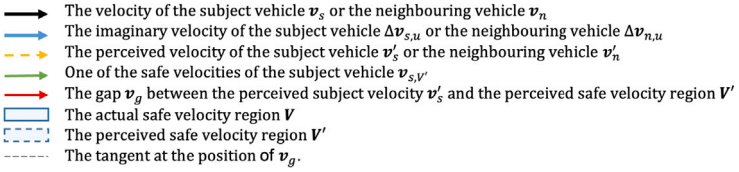

(d) The legend of subfigures (a), (b) and (c)

Fig. 6. An example of the uncertain velocity and its influence on the perceived velocity and the velocity set $\boldsymbol{V}$. The subject vehicle is following a leading vehicle (50 m ahead) with the same velocity $\boldsymbol{v}_s = \boldsymbol{v}_n = 16.67$ m/s and we have the velocity set $\boldsymbol{V}$ according to Eq. (9). In all cases, $\boldsymbol{v}_s \in \boldsymbol{V}$ indicating that the collision avoidance difficulty is originally zero. The velocity $\Delta \boldsymbol{v}_{i,a}$ is not considered due to zero acceleration. This scenario illustrates that uncertainties can cause drivers to perceive vehicle velocities differently from their actual values, which can increase the perceived difficulty of collision avoidance, and thus, perceived risk.

Table 3
The key parameters of PCAD model.

Parameters	Explanations
$\sigma_{i,X}$, $\sigma_{i,Y}$	Standard deviations for uncertain velocity distributions of the subject ($i = s$) and neighbouring ($i = n$) vehicles
$t_{i,a}$	An anticipated time for acceleration-based velocity of the subject ($i = s$) and neighbouring ($i = n$) vehicles
α	The exponent of the velocity weighting function

Accordingly, the uncertain velocity is

$$\Delta \boldsymbol{v}_{i,u} = E(\|\Delta \boldsymbol{v}_{i,u}\|) \cdot \frac{\boldsymbol{p}_s - \boldsymbol{p}_n}{\|\boldsymbol{p}_s - \boldsymbol{p}_n\|} \cdot r_i, \quad i \in \{s, n\}, \quad r_n = 1 \quad \text{and} \quad r_s = -1. \tag{17}$$

Note that this uncertain velocity is not the most probable one but it is the probabilistic average in the most dangerous direction. Although the integral is expressed in an analytical format, *integral* function is used in MATLAB for numerical evaluation.

3.5. Weighting function $\mathcal{W}$

The subject velocity significantly influences perceived risk, as it affects the accident rate and the consequence of a crash. The relationship between velocity and crash outcome is related to the kinetic energy ($E_k = \frac{1}{2}mv^2$) released during a collision but the relationship is not a simple linear mapping. A scaling function ranging on [0, 1] is needed to show the relationship between the subject velocity and perceived risk. Previous studies tried to examine the relationship between the subject velocity and the crash outcome based on real-world crash data and found that a power function best fits the relationship (Aarts and Van Schagen, 2006). We employ a power function proposed by Finch et al. (1994) to describe such a relationship:

$$\mathcal{W} = \beta \left(\frac{\|\boldsymbol{v}_s\|}{v_{\text{ref}}} \right)^{\alpha} \tag{18}$$

where $\|\boldsymbol{v}_s\|$ is the subject velocity; v_{ref} is a reference velocity and it can be set as the velocity limit in specific conditions; α is the power coefficient. This equation also takes into account the mass ratio between neighbouring and subject vehicle. A heavier and larger vehicle will induce a higher perceived risk as it will yield higher subject vehicle accelerations in case of impact. Building upon the PPDRF (Mullakkal-Babu et al., 2020) we introduce the additional scaling $\beta = \frac{M_n}{M_s + M_n}$ where; M_s and M_n are the mass of the subject vehicle and the neighbouring vehicle. Given a speed limit in a specific scenario and a specific vehicle type, the $\mathcal{W} \propto v_s^{\alpha}$ ranging on $[0, 1]$ if $\|\boldsymbol{v}_s\|$ stays below v_{ref}, which can be used as a weight for the final perceived risk based on functions $\mathcal{A}$ and $\mathcal{V}$ as shown in Eq. (1).

3.6. PCAD model parameters

Table 3 summarises the parameters of the PCAD model to be calibrated. Details regarding the avoidance difficulty function $\mathcal{A}$, the perceived velocity function $\mathcal{V}$, and the weighting function $\mathcal{W}$ can be found in Section 3.3, Section 3.4, and Section 3.5, respectively.

4. Analytical model properties

This section offers an analysis of the PCAD model and the three baseline models. Table 2 in Section 2.2 summarises model properties, covering aspects such as dimension, the usage of distance, relative motion, acceleration, subject speed, manoeuvre uncertainties, crash consequences, and usability on curved lanes. In summary, PCAD is a comprehensive model based on Risk Allostasis Theory which considers all aspects listed in Table 2. It is a 2-D model capturing both longitudinal and lateral perceived risk, and can also be used on curved lanes.

For an intuitive understanding, we visualise the perceived risk variations of the four models in a 2-D coordinate system describing the relative position of a neighbouring vehicle. As demonstrated in Fig. 7, perceived risk varies with different relative velocities (Fig. 7(b)), different decelerations (Fig. 7(c)), and different subject velocities (Fig. 7(d)). Fig. 7(a) provides the legend for these diagrams.

The PCAD model indicates that perceived risk amplifies as an object or neighbouring vehicle nears the subject vehicle, demonstrating a sharp rise both longitudinally and laterally. The non-linear relationship caused by non-linear *looming detection* in PCAD prevails in the other three typical models but is described by different functions such as Gaussian (i.g., the lateral risk in PPDRF and DRF), Exponential (i.g., the potential risk in PPDRF), logarithmic (i.g., the risk in RPR) and Quadratic functions (i.g., the longitudinal risk in DRF). Note that RPR cannot capture perceived risk in the lateral direction since it is only defined in the same traffic lane.

PCAD shows that human drivers perceive more risk when approaching an object faster. Compared to the other three models, PCAD and PPDRF can output different perceived risk values facing different relative velocities (Fig. 7(b)). RPR and DRF do not include velocity information of the neighbouring vehicles or objects.

Reacting to neighbouring vehicles' velocity changes (e.g., braking) is a common task in daily driving. PCAD can clearly describe effects on perceived risk (Fig. 7(c)) where $a_n = -8\,\mathrm{m/s^2}$ leads to the highest perceived risk and $a_n = 0$ causes the lowest perceived risk. RPR and PPDRF also capture effects of acceleration but DRF cannot indicate the change of perceived risk caused by a neighbouring vehicle's deceleration due to a lack of acceleration information in the model.

The subject velocity significantly influences perceived risk. In Fig. 7(d), PCAD demonstrates that, given the same following gap, human drivers perceive more risk with a higher subject velocity, which is similar to PPDRF and DRF. However, RPR does not contain subject speed information in the model and cannot capture the perceived risk variance in this condition.

5. Model evaluation method

To conduct a comparative evaluation of the proposed model and the baseline models, model calibration with empirical data is indispensable. This section details the experimental datasets, calibration method, and performance indices for the models.

5.1. Dataset introduction

We employ two datasets for model calibration and evaluation. The first dataset (**Dataset Merging**) was collected in our previous simulator experiment where the subject automated vehicle reacts to merging and hard-braking vehicles. The experiment simulated 18 merging event types with different merging distances and braking intensities on a 2-lane highway (He et al., 2022). Fig. 8 shows an example of the simulated events during the experiment. The participants were asked to monitor the scenario as fall-back ready drivers for an SAE Level 2 automated vehicle. They used a pressure sensor on the steering wheel to provide perceived risk ratings from 0–10 continuously in the time domain (see the lower row in Fig. 8), which are the continuous perceived risk data. After each event, the participants were also asked to give a verbal perceived risk rating from 0–10 regarding the previous event, which is the discrete event-based perceived risk data. The corresponding kinematic data (e.g. position, speed and acceleration of the subject vehicle and neighbouring vehicles) were collected simultaneously.

The second dataset (**Dataset Obstacle Avoidance**) includes drivers' verbal perceived risk ratings (i.e., unlimited numbers) and steering angle signals when the participants face static obstacles suddenly appearing in front the subject vehicle driving at $25\,\mathrm{m/s}$ in manual driving mode (Kolekar et al., 2020b). Fig. 9 shows the distribution of the obstacles. The corresponding vehicle kinematic data and the positions of the obstacles were recorded at the same time.

The following reference data is utilised for model calibration:

- Dataset Merging: the **event-based perceived risk rating** and the **peak of the continuous perceived risk** in specific events
- Dataset Obstacle Avoidance: the **event-based perceived risk**, and the **peak of steering wheel angle** in specific events

Figs. B.14 and B.15 in Appendix B illustrate the kinematic data from the two datasets, along with the continuous risk predicted by PCAD.

5.2. Model calibration

While our aim is to develop general models considering the average characteristics of all participants, we cannot ignore the influence of group features and scenarios. To optimise performance, we perform a dataset-level calibration of parameters for all models. We have $RMSE_i$ defined as

$$RMSE_q = \sqrt{\frac{\sum_{k=1}^{K}\left(\hat{y}_k - y_k\right)^2}{K}} \tag{19}$$

Here, $RMSE_q$ denotes the root mean square error between the collected perceived risk data and the model output. For Dataset Merging, $q = event$ and $q = peak$ represent the $RMSE$ for event-based perceived risk and the peak of continuous perceived risk respectively; for Dataset Obstacle Avoidance, $q = event$ and $q = peak$ denote the $RMSE$ for event-based perceived risk and the maximum steering wheel angle separately. In Eq. (19), $\hat{y}_k$ represents the model output, while y_k refers to the perceived risk rating. The variable k, which falls within the set of $1, 2, 3, \ldots, K$, represents the event number in the specific dataset. K signifies the number of available events in different datasets, with $K = 414$ for Dataset Merging and $K = 2496$ for Dataset Obstacle Avoidance. Note that the first sample point of the kinematic data when the obstacle suddenly appears in Dataset Obstacle Avoidance is used for the calibration since the participants were asked to give a verbal perceived risk rating as soon as the obstacle appeared.

The calibration aims to minimise $\sum RMSE_q$ for all models by tuning the key model parameters based on perceived risk and corresponding kinematic data. Given the variability in perceived risk data ranges across the two datasets and the differing output ranges of the four models, min–max feature scaling is employed to normalise both perceived risk data and model outputs to a uniform range of [0, 10]. This normalisation facilitates direct comparison and calibration, as encapsulated in Eq. (20).

$$\hat{z}_k = \frac{z_k - z_{\min}}{z_{\max} - z_{\min}} \times 10 \tag{20}$$

where $\hat{z}_k$ represents the scaled value, either model output or perceived risk data. For model outputs, $z_{\max}$ and $z_{\min}$ are the global maximum and minimum values across all outputs for a specific model per dataset. In contrast, for perceived risk ratings within the Dataset Obstacle Avoidance, the scaling is conducted individually for each participant, reflecting the participant-specific range of

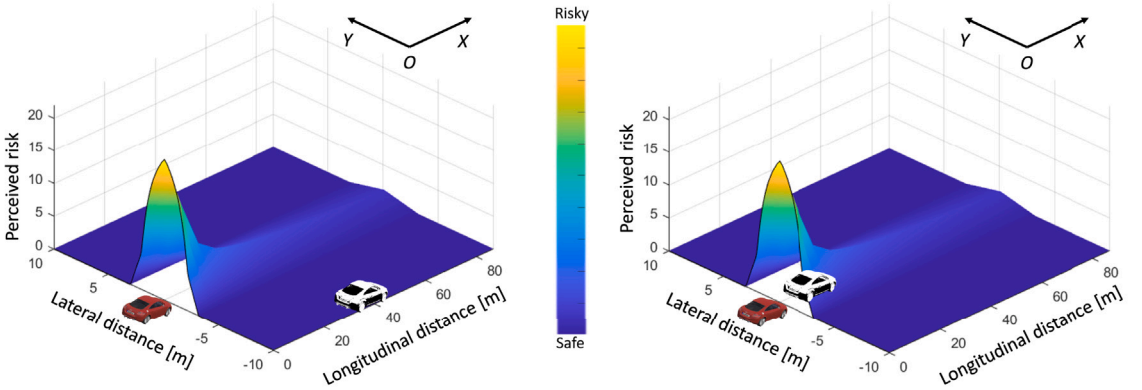

(a) Legend and explanation of figures (b), (c), (d). Surfaces represent the computed perceived risk value of different models as function of the relative 2D position of the subject vehicle (red) and neighbouring vehicle (white). The subject vehicle is at the origin $(0,0)$, moving with velocity $\boldsymbol{v}_{s,X} = 100\,\text{km/h}$ along the X-axis. The neighbouring vehicle's velocity is $\boldsymbol{v}_{n,X} = 50\,\text{km/h}$, also along the X-axis. In the left figure, the neighbouring vehicle at $(40,-10)$ implies a front-right position relative to the subject vehicle, indicating low perceived risk. In the right figure, the neighbouring vehicle at $(10,0)$ shows the subject vehicle approaching the leader with a relative velocity $\boldsymbol{\Delta v} = \boldsymbol{v}_{s,X} - \boldsymbol{v}_{n,X} = 50\,\text{km/h}$ and a longitudinal gap of $10\,\text{m}$, resulting in high perceived risk.

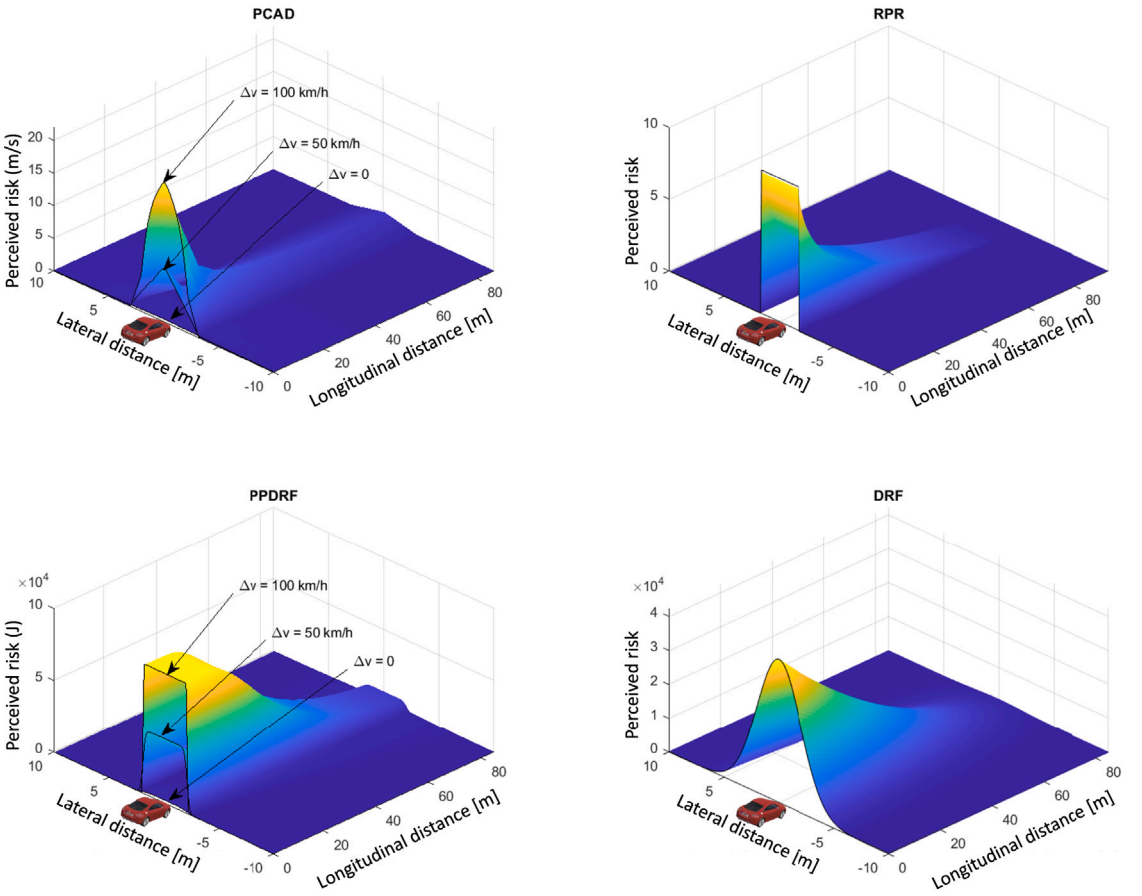

(b) The effect of relative velocity on human driver's perceived risk. The constant subject vehicle velocity is $v_{s,X}$ = 100 km/h but the neighbouring vehicle has different velocities $v_{n,X}$; no acceleration of the subject vehicle and the neighbouring vehicle $a_{s,X} = a_{n,X} = 0$. Note that PPDRF's kinetic risk instead of potential risk is used here for a more understandable visualisation.

Fig. 7. The effect of relative velocity (b), the acceleration of the neighbouring vehicle (c) and the subject velocity (d) with legend in (a).

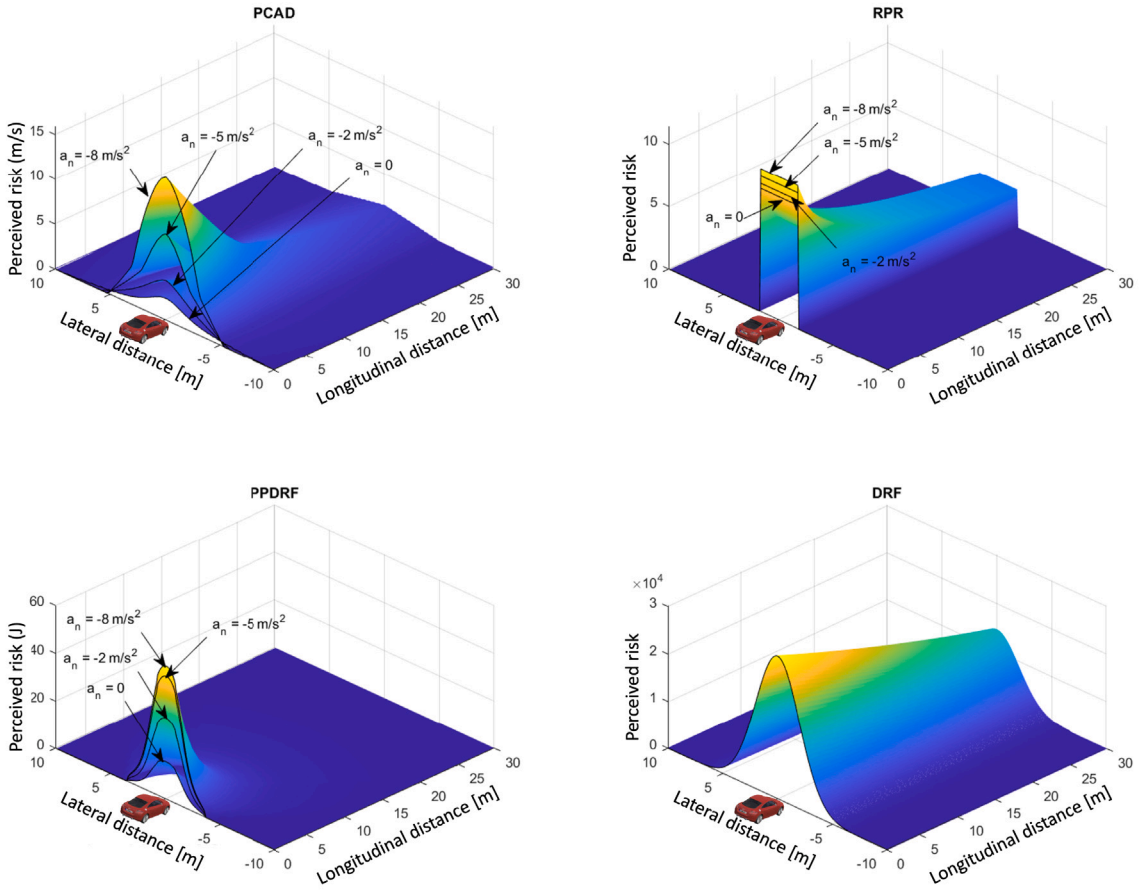

(c) The effect of neighbouring vehicle's known acceleration (braking) on human driver's perceived risk. The velocity of the subject vehicle and the neighbouring vehicle are equal $v_{s,X} = v_{n,X} = 100$ km/h; the subject vehicle has no acceleration $a_{s,X} = 0$ but the neighbouring vehicle's known acceleration ($a_{n,X}$) varies.

Fig. 7. (*continued*).

ratings. This distinction is crucial, as it allows for the individual scaling of perceived risk ratings in the Dataset Obstacle Avoidance due to its unrestricted numerical range and participant-specific variation, while maintaining a universal scaling framework for model outputs and the already bounded ratings with the range [0, 10] in Dataset Merging.

This scaling approach ensures that both participant-specific variations in perceived risk assessment and the diverse output ranges of different models are appropriately normalised for accurate calibration and comparison.

5.3. Performance indicators

We use five indicators to evaluate the model performance: Correlation, Model error, Detection rate, Computation cost, and Linear Time Scaling Factor.

- **Correlation** The predicted perceived risk has to be correlated with the event-based perceived risk. We use R-Square to quantify how well model outputs fit the real perceived risk. Since the perceived risk output by the models is linearly rescaled to 0–10 (Eq. (20)), different ranges of perceived risk data or model outputs have no influence on R-Square in our case.
- **Model error** We use Root Mean Squared Error (RMSE) to quantify a model's overall Model error, which is the same as the model calibration criterion (Eq. (19)). This indicator reflects the model's ability to compute the overall perceived risk in a certain dataset. A model with a smaller $RMSE$ can more accurately predict the overall perceived risk for a given scenario.

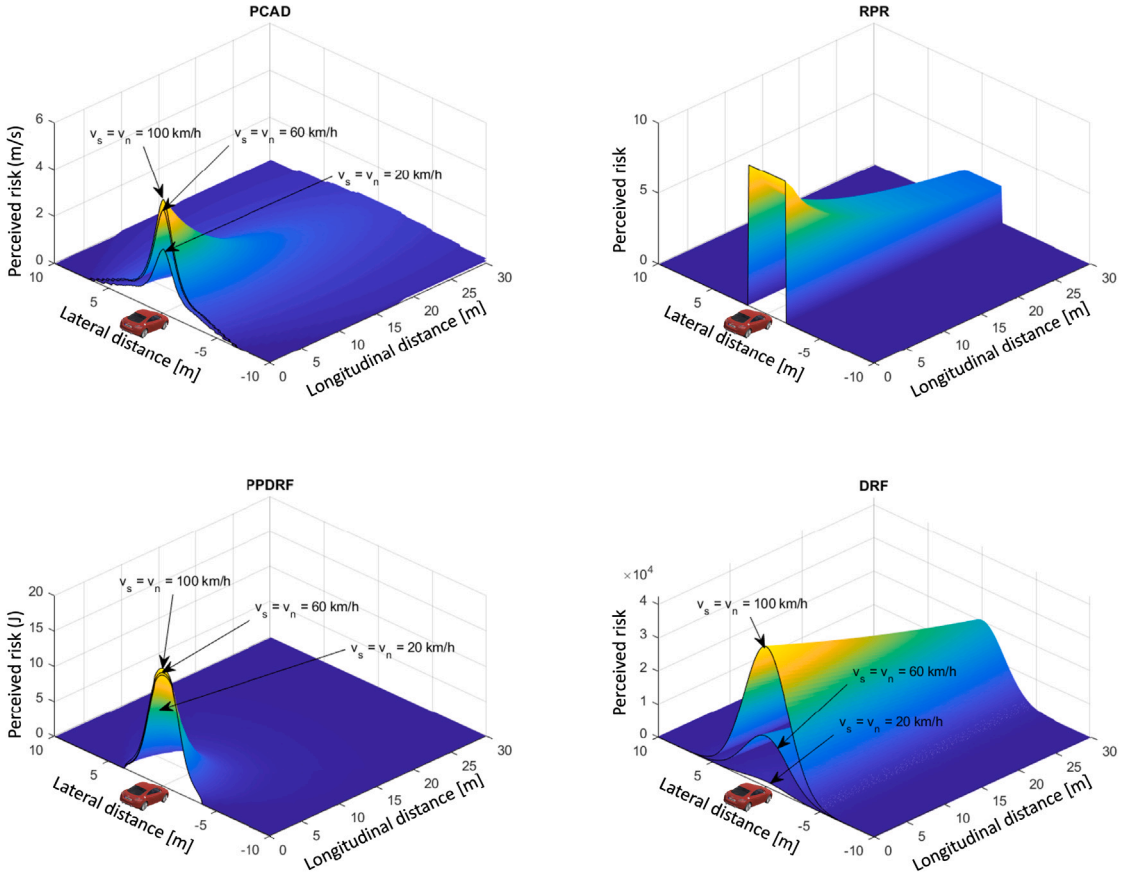

(d) The effect of subject velocity. Human driver's perceived risk. The subject vehicle and the neighbouring vehicle have equal velocity ($v_{s,X} = v_{n,X}$) varying from 20 km/h-100 km/h; no acceleration of the subject vehicle and the neighbouring vehicle $a_{s,X} = a_{n,X} = 0$.

Fig. 7. (*continued*).

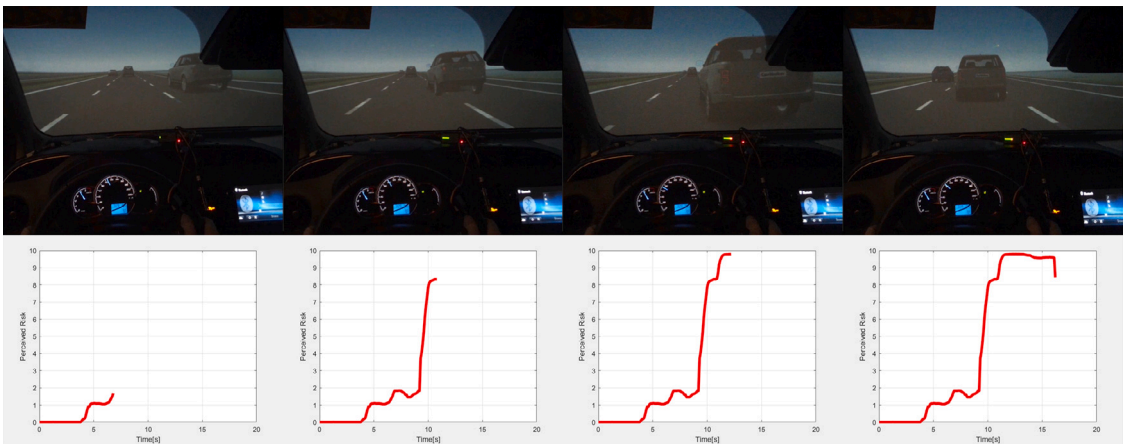

Fig. 8. The experiment where Dataset Merging was collected. Upper row: Video stream of a merging with hard braking event simulated in the experiment. Lower row: Corresponding perceived risk values indicated by a participant with the pressure sensor.

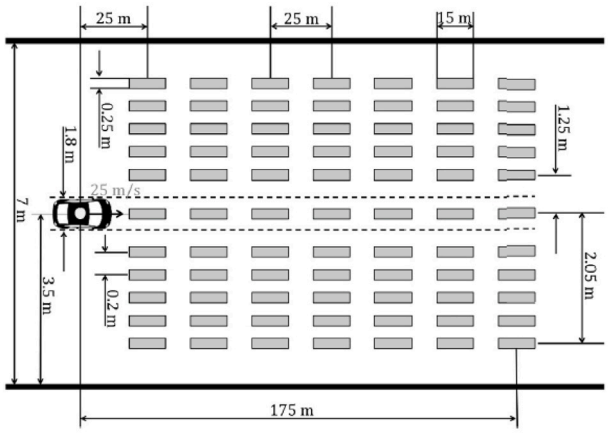

Fig. 9. Dataset Obstacle Avoidance, with stationary obstacle positions from Kolekar et al. (2020b).

- **Detection rate** The Detection rate represents the model's ability to detect an event's risk that is also perceived by human drivers. We defined Detection rate as in Eq. (21)

$$R_{det} = \frac{K_{detected}}{K_{event}} \times 100\% \tag{21}$$

  where $K_{detected}$ represents the number of events where the model manages to detect the risk with non-zero output; K_{event} is the total number of the events where human drivers gave perceived risk ratings in a certain dataset with $K_{event} = 414$ for Dataset Merging and $K_{event} = 2496$ for Dataset Obstacle Avoidance. In this study, every event carries a 'risk' due to experimental settings, which simulate scenarios where some level of risk is always present. Consequently, the detection of an event, reflected by a non-zero output, implies the recognition of this risk. Therefore, a higher detection rate correlates with better model performance, as it indicates the model's consistent ability to recognise the presence of risk in every event.
- **Computation cost** It is essential that all models possess real-time risk computation capability, so the computation cost is critical. More complex models may offer a better performance in other aspects such as model errors but tend to take longer to compute. We define the computation cost as the model's computation time per computation step. If the time consumption per computation step exceeds the on-board computation capability, it means that the computation of perceived risk cannot be completed in real-time.

The above metrics validate the event-based perceived risk. We also compared the continuous perceived risk measured for Dataset Merging. However, we observed that participants pressed the button following a fixed pattern regardless of the actual real-time risk level. This suggests that the timing of their responses was more likely influenced by the given instructions and their interpretation, rather than reflecting a valid measure of continuous perceived risk over time. Consequently, these responses, although appearing as a 'continuous perceived risk', do not offer reliable time-domain information. Due to this lack of time-domain validation, we have chosen not to report on the validation of continuous perceived risk.

6. Model evaluation results

In this section, we illustrate the applicability of the four models and evaluate their performance with the performance indicators introduced previously regarding the two datasets.

6.1. Model calibration results

The calibration is performed separately for the two datasets. According to the model structure and dataset features, the calibrated parameters are listed in Table 4.

6.2. Performance evaluation results

We test the four models using both datasets including the perceived risk data and the corresponding kinematic data with the calibrated parameters shown in Table 4. The following sections present different aspects of performance.

6.2.1. Correlation

The correlation between predicted and measured event-based perceived risk data plays a crucial role in assessing the performance of risk assessment models. This is particularly important given the uncertainty in defining the unit of perceived risk. Fig. 10 and Fig. 11 display the correlation between the predicted perceived risk and event-based perceived risk for Dataset Merging and Dataset Obstacle Avoidance respectively. The adjusted R-Square is calculated based on the averaged event-based perceived risk across the same event type (● in Figs. 10 and 11).

In both datasets, the PCAD model demonstrates a superior correlation with event-based perceived risk data compared to other models. Furthermore, the regression models RPR and DRF exhibit strong performance in Dataset Merging and Dataset Obstacle Avoidance, respectively, for which they were originally developed.

6.2.2. Model error

As discussed in Section 5.3, the Root Mean Square Error ($RMSE$) is an indicator of the overall Model error. Table 5 presents the RMSE values for all four models across the two datasets.

The $RMSE$ values (both event and peak) reveal that the PCAD model achieves a comparable performance level to the regression models (e.g., RPR in Dataset Merging and DRF in Dataset Obstacle Avoidance), albeit with a slightly larger model error. In Dataset Merging, the lower $RMSE$ values for PCAD and RPR suggest better performance, as these models directly incorporate the neighbouring vehicle's acceleration. In Dataset Obstacle Avoidance, the lower $RMSE$ values for PCAD and DRF indicate superior performance, as these models also consider lateral perceived risk, resulting in reduced model error when applied to a 2-D dataset (Table 5). The PPDRF model was originally designed to evaluate actual collision risk in traffic, and was not previously calibrated or validated. We now performed such a calibration and demonstrate moderate performance in both datasets.

6.2.3. Detection rate

As per Eq. (21), the detection rates for the four models across both datasets are presented in Table 5. In Dataset Merging, the merging vehicle primarily poses longitudinal risk in the same lane. Consequently, all models are capable of detecting dangerous events, regardless of whether they are 1-D or 2-D models. However, in Dataset Obstacle Avoidance, the obstacles are dispersed across a 2-D plane. As a result, only models that account for lateral risk can effectively identify dangerous vehicles outside the forward path. This leads to a lower detection rate for the RPR model, while the other three models are able to recognise all dangerous events that human drivers also perceive as risky. Note that Fig. 11 displays outputs with marginal values that appear to be zero but are, in fact, detected by PPDRF.

6.2.4. Computation cost

Table 5 presents the computation cost for different models, tested on a workstation with an Intel Core i7-8665U 1.9 GHz processor and 8 GB RAM. Generally, models that take more factors into account require longer computation times. In both datasets, RPR is the fastest model, as it only involves logarithmic calculations.

In Dataset Merging, PCAD is the most time-consuming model since it relies on a grid search to identify the optimal velocity gap vector to the safe velocity region. PPDRF requires spatial overlap computations and multiple integrals over variations of acceleration probability density function in the overlap area, making it a time-intensive process. Although DRF involves discretising a 2D area of an object or a vehicle with a grid and summing the risk values over each grid cell to obtain the final perceived risk, its overlap computations are simpler than those of PPDRF, as the risk field and severity field are static and no motion prediction of neighbouring vehicles is needed.

In Dataset Obstacle Avoidance, PPDRF takes less time than DRF and PCAD, as it only computes potential risk, which is a simpler process compared to the kinetic risk computation in Dataset Merging.

6.2.5. Summary of model performance evaluation

Based on the results discussed above, we utilise radar charts to illustrate the performance of each model across various aspects, as shown in Fig. 12. Generally, PCAD demonstrates strong performance in terms of overall model error, R-square, and detection rate. However, the primary drawback of PCAD is its high computation cost, which results from its complexity. The regression models (i.e., RPR in Dataset Merging and DRF in Obstacle Avoidance) exhibit the best performance in their respective datasets. We remark that the advantage of PPDRF in capturing the manoeuvre uncertainties of the surrounding vehicles vanishes in the second dataset due to the specific experimental setting. As a result, the PPDRF models used in the two datasets are two different models. This largely explains the poor performance of PPDRF, albeit it clearly showed advantages in the analytical model properties.

It is worth mentioning that PCAD demonstrates excellent and consistent performance across both datasets. We also conducted cross-validation between the two datasets, in which the four models and their parameters were calibrated using one dataset and then used to predict perceived risk in the other dataset. PCAD performs quite well even without re-calibration where as seen in Table C.6, Figs. C.16–C.18 in Appendix C, PCAD maintains its strong performance in cross-validation. Additionally, this suggests that the calibration process has a low risk of overfitting, further highlighting the robustness of the PCAD model.

Table 4
Calibrated parameters for all models.

Model	Parameters	Explanation	Values for dataset merging	Values for dataset obstacle avoidance
PCAD[a]	$\sigma_{n,X}$	The standard deviation in X of the velocity Gaussian of a neighbouring vehicle (m/s)	4.28	/
	$\sigma_{n,Y}$	The standard deviation in Y of the velocity Gaussian of a neighbouring vehicle (m/s)	3.86	/
	$\sigma_{s,X}$	The standard deviation in X of the velocity Gaussian of the subject vehicle (m/s)	0.80	6.58
	$\sigma_{s,Y}$	The standard deviation in Y of the velocity Gaussian of the subject vehicle (m/s)	1.70	1.20
	$t_{s,a}$	The anticipated time for the acceleration-based velocity of the subject vehicle (s)	0.13	/
	$t_{n,a}$	The anticipated time for the acceleration-based velocity of a neighbouring vehicle (s)	0.01	/
	α	The exponent of the power function in velocity weighting function	0.52[b]	/
RPR	C_0	The intercept in the regression model	12.10	20.70
	C_1	The coefficient of gap to the leading vehicle	−3.70	−3.68
	C_2	The coefficient of leading vehicle's braking intensity	−0.36	/
PPDRF	$\tilde{\sigma}_x$	The standard deviation of longitudinal acceleration distribution of neighbouring vehicle (m/s^2)	2.01	/
	$\tilde{\sigma}_y$	The standard deviation of lateral acceleration distribution of neighbouring vehicle (m/s^2)	0.02	/
	D	The steepness of descent of the potential field	/	0.14
DRF[c]	s	The steepness of the height parabola of the risk field	0.15	0.005
	t_{la}	Human driver's preview time (s)	1.20	8.12
	m	The rate of the risk field width expanding	3.98×10^{-8}	3.66×10^{-4}
	c	The initial width of the DRF (m)	0.45	1.10

[a] The experimental design of two datasets, featuring only one category of obstacle or other road users, means that the mass ratio β remains constant. Consequently, in the calibration phase, this ratio is set to 1.

[b] This is the calibrated value regarding the specific dataset. Due to the lack of subject velocity change, α has limited influence on Dataset Merging. α ranging on [0, 2.5] leads to an R-square ranging on [0.80, 0.90]. For Dataset Obstacle Avoidance, α was set to 0 since it almost has no influence. Additionally, the v_{ref} in the weighting function $\mathcal{W}$ was set to 27.78 m/s for Dataset Merging and 25 m/s for Dataset Obstacle Avoidance.

[c] The best performance for DRF was obtained when the subject velocity $\boldsymbol{v}_{s,X}$ in Eq. (A.9) was fixed to its initial value 27.78 m/s when the vehicle decelerated for Dataset Merging. For Dataset Obstacle Avoidance, the subject velocity $\boldsymbol{v}_{s,X}$ was a constant 25 m/s.

Table 5
Model performance represented by the performance indicators.

Dataset	Performance indicators	PCAD	RPR	PPDRF	DRF
Dataset Merging	$RMSE_{event}$	2.25	2.18	2.76	2.58
	$RMSE_{peak}$	3.41	3.39	3.73	3.35
	Adjusted R-Square	0.90	0.90	0.90	0.67
	Detection rate	1.00	1.00	1.00	1.00
	Computation cost (ms)[a]	2.79	1.77×10^{-4}	6.14[e]	1.30
Dataset Obstacle Avoidance	$RMSE_{event}$	2.27	3.20	3.34	2.17
	$RMSE_{peak}$	2.71	3.84	4.02	2.61
	Adjusted R-Square	0.90	0.38	0.50	0.90
	Detection rate	1.00	0.09[d]	1.00	1.00
	Computation cost (ms)[b]	6.70[c]	2.01×10^{-4}	1.08×10^{-2}	1.22

[a] The average value of computing 124614 steps.

[b] The average value of computing 349440 steps.

[c] PCAD consumed more time in Dataset Obstacle Avoidance because the searching algorithm worked in a larger searching area to find the velocity gap $\boldsymbol{v}_g$.

[d] Only the vehicles directly in front of the vehicle can be detected by RPR, which leads to a low detection rate. See Kolekar et al. (2020b) for more experiment details.

[e] PPDRF consumed much more time in Dataset Merging because the model contains numerical integration when facing moving vehicles.

7. Discussion

In this paper, we present a computational perceived risk model based on the Risk Allostasis Theory (Fuller, 1984, 1999, 2011), capturing task difficulty using the gap between the current velocity and the safe velocity region in 2D. Our model quantifies event-based perceived risk and the peak of continuous perceived risk in both longitudinal and lateral directions. We validated the model on two datasets of human drivers' perceived risk and compared its performance with three baseline perceived risk models. Our work contributes to addressing the challenge of perceived risk computation for SAE Level 2 driving automation, while also illustrating the mechanisms underlying human drivers' risk perception.

Traditional perceived risk models consider collision probability and the collision consequence (Näätänen and Summala, 1976), such as DRF and PPDRF, while our PCAD model is developed based on the concept of potential collision judgement using looming, which originates from aerospace and maritime experience (Ward et al., 2015). PCAD demonstrates superior performance in estimating perceived risk in various driving conditions, aligning with the argument of McKenna (1982), Rundmo and Nordfjærn (2017) that drivers are incapable of monitoring infrequent event probabilities, thus supporting the underlying theory of PCAD.

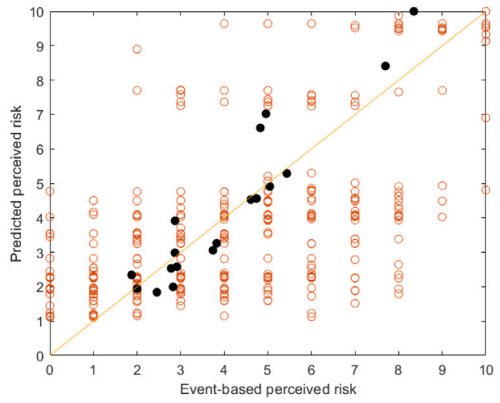

(a) PCAD (Adjusted R-Square = 0.90)

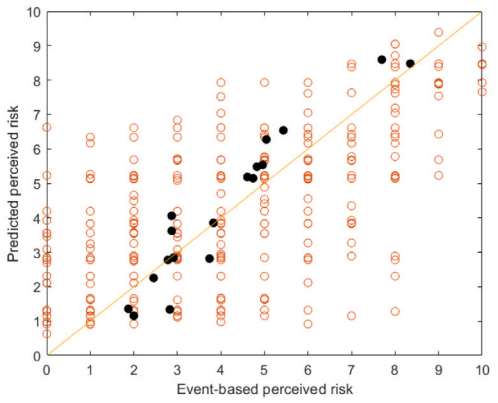

(b) RPR (Adjusted R-Square = 0.90)

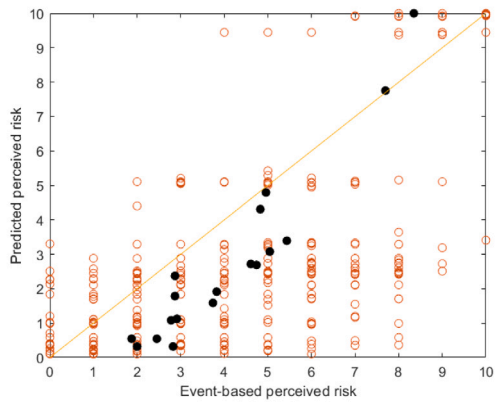

(c) PPDRF (Adjusted R-Square = 0.90)

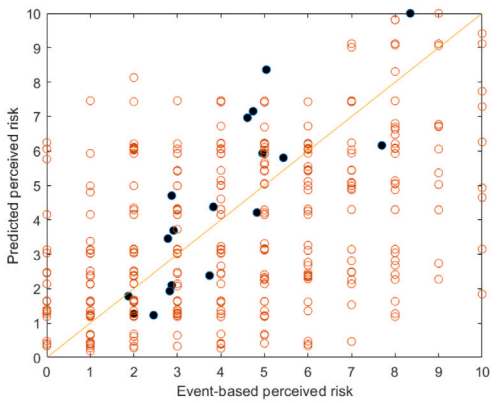

(d) DRF (Adjusted R-Square = 0.67)

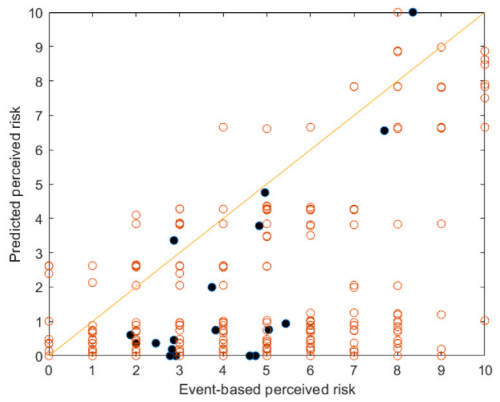

(e) PCAD with only deterministic motion information (Adjusted R-Square = 0.58)

Fig. 10. Predicted and measured event-based perceived risk in Dataset Merging. "○" indicates individual event-based perceived risk and "●" indicates the averaged event-based perceived risk across the same event type, for which the Adjusted R-Square is also given.

The demonstrated superior performance of our PCAD model unveils new insights into perceived risk. Firstly, PCAD considers all motion information in Table 2, highlighting the importance of position, velocity, and acceleration for risk perception. Secondly, the models that can capture lateral risk lead to a higher detection rate in Dataset Obstacle Avoidance, indicating that perceived risk is 2-D and human drivers perceive the risk from all directions in a 2-D plane. Thirdly, manoeuvre uncertainties of the subject vehicle and other road users cause extra perceived risk, which is supported by Kolekar et al. (2020b) and Ding et al. (2014). Lastly,

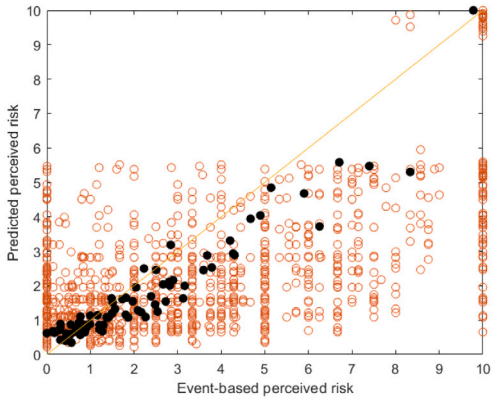

(a) PCAD (Adjusted R-Square = 0.90)

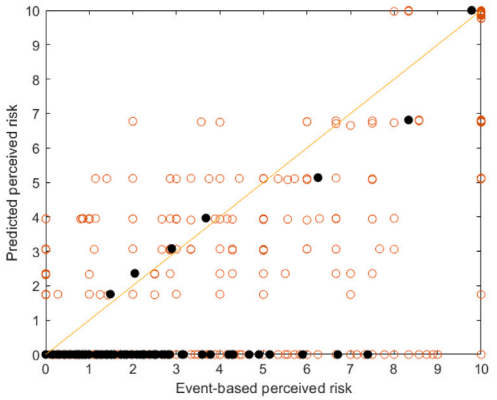

(b) RPR (Adjusted R-Square = 0.38)

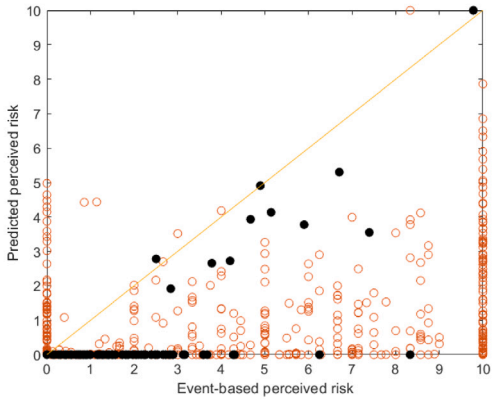

(c) PPDRF (Adjusted R-Square = 0.50)

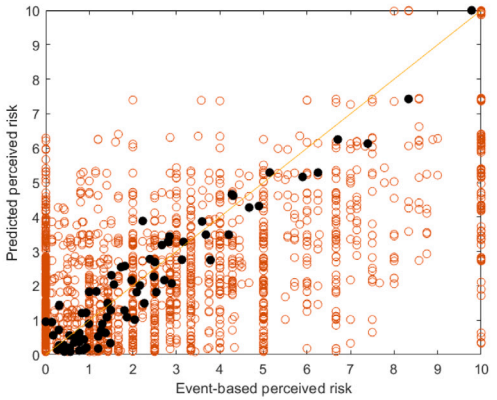

(d) DRF (Adjusted R-Square = 0.90)

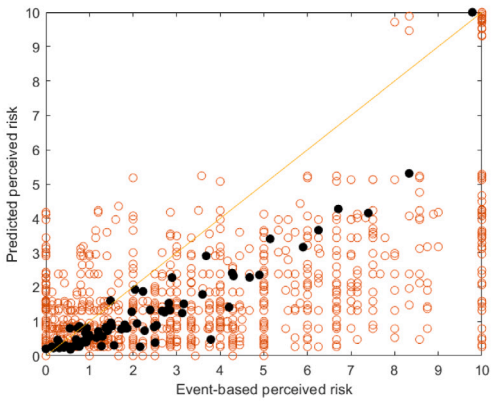

(e) PCAD with only deterministic motion information (Adjusted R-Square = 0.81)

Fig. 11. Predicted and measured event-based perceived risk in Dataset Obstacle Avoidance. "○" indicates individual event-based perceived risk and "●" indicates the averaged event-based perceived risk across the same event type. Note that in (c), there are many dots with small values but non-zero, indicating that they are actually detected by PPDRF.

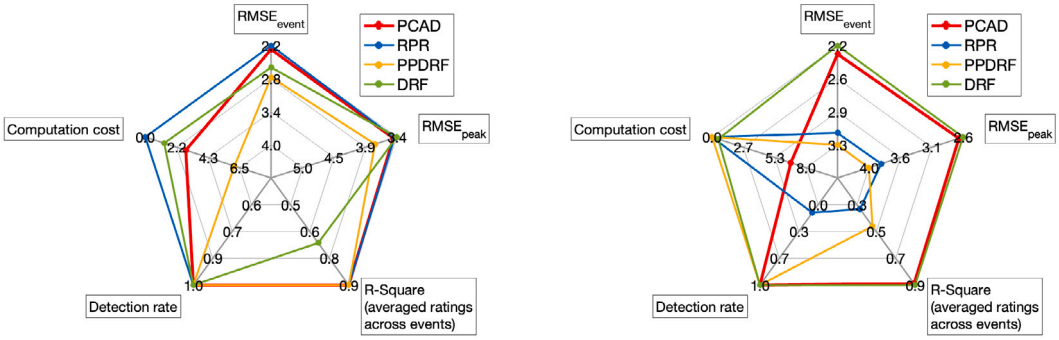

(a) Performances in Dataset Merging

(b) Performances in Dataset Obstacle Avoidance

Fig. 12. Radar charts of model performance indicators in two datasets.

perceived risk is a dynamic concept and varies with the changing traffic conditions as illustrated in Fig. 7, which presents the perceived risk variations in three distinct driving conditions (i.g., different relative velocities, subject velocities and accelerations). This observation motivates the need for models, such as the proposed PCAD model, which can adjust to varying driving scenarios even without recalibration.

It is plausible that drivers associate trucks with higher threats compared to cars, and tend to maintain greater distances accordingly. Our model incorporates this by adjusting perceived risk levels to the mass ratio. Furthermore, the distance between reference points on neighbouring vehicles also affects the model's output. A larger vehicle like a heavy truck will have reference points that are farther apart, resulting in a smaller safe velocity set and consequently, a higher perceived risk. Our model can thus explain the cautious behaviour when driving around trucks, which can lead to more realistic assessment of perceived risk.

We note that our model has limitations. There is only one traffic object considered in this study. If multi-road users or even infrastructure is added, PCAD still has the potential to estimate perceived risk. In that case, we need to compute the potential collision avoidance difficulty for multiple neighbouring vehicles considering them simultaneously. Based on this we can calculate the comprehensive safe velocity set and derive the total perceived risk.

The PCAD model's identification of the minimal velocity change $\boldsymbol{v}_g$ does not account for drivers' tendency to assign different weights to braking and steering based on the driving experience and situational complexity. This anisotropic weighting in driver's decision-making is not captured by the current model. Exploring this difference presents a potential opportunity to improve the PCAD model to more accurately simulate real-world driver behaviour and improve its applicability in safety-critical scenarios.

It is important to acknowledge that integrating advanced motion prediction techniques into models assessing collision avoidance and perceived risk undoubtedly enhances their predictive accuracy. Our model, within its current scope, incorporates aspects of motion prediction through the inclusion of acceleration-based velocity and uncertain velocity, offering a simplified but effective approach to understanding driving dynamics. The primary objective of this research has been to establish a foundational model capable of predicting perceived risk via collision avoidance difficulty. This aim has shaped our methodological choices, balancing model complexity with practical applicability. While there are limitations associated with the simplified approach to motion prediction, these do not diminish the contributions of our work. Instead, they highlight areas for future research and development, suggesting paths for incorporating more advanced motion prediction methodologies to further enhance the model's precision and usefulness in studies on perceived risk.

Regarding perceived risk data, Dataset Merging covers human driver's perceived risk with SAE Level 2 driving automation where drivers need to monitor the system and environment and be ready to intervene. This makes this data suitable to assess perceived safety when using automation, but the lateral risk is not systematically explored. Dataset Obstacle Avoidance explores human drivers perceived risk data in 2-D, including lateral perceived risk. However, this dataset is collected from human-automation transitions (i.g., human drivers' taking-over process in this case), which may cause bias in automated driving conditions. Additionally, the objects in the experiment are fixed and suddenly displayed during driving. The additional perceived risk caused by surprise cannot be ignored.

Dataset Merging measured perceived risk on a scale from 0 to 10 for no to very high risk, while Dataset Obstacle Avoidance captured perceived risk as a non-negative real number without predetermined upper limit. To facilitate comparison, all results from Dataset Obstacle Avoidance and all models were scaled to 0–10 to match the scale used in Dataset Merging. More specific scales of perceived risk can be developed for experimental studies, including factors such as accident risk and severity, and the driver's tendency or need to intervene and overrule the driving automation.

To further advance perceived risk modelling, we recommend collecting more perceived risk data in various scenarios through online surveys with videos, simulator experiments and on-road observations. Such additional data can help to assess the validity of the PCAD model also in multi-vehicle interactions, and infrastructure interactions including curve negotiation. Additional data

can also serve to examine perceived risk at different driving automation levels. Moreover, internal HMIs have positive effects in reducing human drivers' perceived risk and the perceived risk modelling will be further improved to capture different internal HMI conditions (Kim et al., 2024; Jouhri et al., 2023). Our PCAD model can also be used as a cost function, a constraint, or a reference of perceived risk in driving automation decision making, trajectory planning, or controller design, enhancing trust (Hu and Wang, 2021) and acceptance.

8. Conclusions

In this study, we have formulated, calibrated, and validated a novel computational perceived risk model, and compared its performance with three well-established models across two different datasets. Our findings reveal valuable insights into the understanding and quantification of perceived risk in various driving situations. The key conclusions drawn from our analysis are as follows: (1) Driving task difficulty serves as an effective indicator of perceived risk; (2) Perceived risk is two-dimensional, originating from both longitudinal and lateral directions, and exhibits a non-linear increase as the distance to surrounding vehicles decreases; (3) Incorporating uncertainties in the model is crucial for an accurate representation of perceived risk; (4) Perceived risk is dynamic and changes with driving conditions.

Code availability

The source MATLAB code that helps explain the PCAD model is available for examination and use. It can be found via this link https://doi.org/10.4121/3ad2db22-ea82-4436-8df5-ebbbdb4aeec6. By providing access to this code, we aim to facilitate further development and independent verification of the results, as well as the possibility for its application in related fields.

CRediT authorship contribution statement

Xiaolin He: Writing – review & editing, Writing – original draft, Visualization, Validation, Software, Methodology, Formal analysis, Data curation, Conceptualization. **Riender Happee:** Writing – review & editing, Supervision, Project administration, Methodology, Funding acquisition, Conceptualization. **Meng Wang:** Writing – review & editing, Supervision, Project administration, Methodology, Conceptualization.

Declaration of competing interest

The authors declare that they have no known competing financial interests or personal relationships that could have appeared to influence the work reported in this paper.

Data availability

The source MATLAB code that helps explain the PCAD model is available for examination and use. It can be found via this link https://doi.org/10.4121/3ad2db22-ea82-4436-8df5-ebbbdb4aeec6. By providing access to this code, we aim to facilitate further development and independent verification of the results, as well as the possibility for its application in related fields.

Acknowledgements

This research is supported by the SHAPE-IT project funded by the European Union's Horizon 2020 research and innovation programme under the Marie Skłodowska-Curie grant agreement 860410. The authors also would like to thank Toyota Motor Europe NV/SA for the support in conducting the simulator experiment and model validation.

Appendix A. Related perceived risk models

A.1. Regression Perceived Risk Model (RPR)

The Regression Perceived Risk model (RPR) is an event-based perceived risk model derived from our previous simulator experiment, where 18 merging events with various merging distances and braking intensities on a 2-lane highway were simulated. RPR predicts human drivers' event-based perceived risk ratings ranging from 0–10 regarding merging events based on the corresponding kinematic data from the simulator drive.

The RPR model builds on several assumptions:

- Perceived risk stems from the vehicles directly in front of the subject vehicle, which means the merging vehicles cause perceived risk only after entering the current lane.
- Drivers can accurately estimate the motion information (e.g., relative position, velocity, acceleration, etc.) with the human sensory system.

The initial model can predict event-based perceived risk (He et al., 2022), as shown in Eq. (A.1)

$$R_{RPR\_event} = 9.384 - 2.473 \cdot \ln(gap_{min}) - 0.038 \cdot YDL - 0.201 \cdot BI_{max} + 0.470 \cdot GEN \tag{A.1}$$

where R_{RPR_event} is the event-based perceived risk ranging from 0–10; gap_{min} is the minimum clearance in metres to the leading vehicle during an event; YDL represents the years with a valid driving licence; BI_{max} denotes the maximum braking intensity (m/s^2) of the merging vehicle; GEN represents the gender of the participants with $Female = 1$ and $Male = 0$. The model coefficients were originally calibrated based on a perceived risk dataset (He et al., 2022), detailed in Section 5.1.

We extend the model to compute real-time perceived risk by replacing min_gap and max_BI with the real-time values. YDL and GEN are omitted since they remain constant for a certain group of participants, and can be accounted for by the intercept. In this way, RPR is formulated in the continuous time domain as

$$R_{RPR}(t) = C_0 + C_1 \cdot \ln(x_n(t) - x_s(t)) + C_2 \cdot a_{n,X}(t) \tag{A.2}$$

where $x_n(t)$ and $x_s(t)$ are the real-time longitudinal position (m) of the neighbouring vehicle and the subject vehicle; $a_{n,X}(t)$ is the current acceleration (m/s^2) of the neighbouring vehicle, which is the braking intensity in this model; According to the simulator experiment settings (He et al., 2022), the validity range of the model is that $x_n(t) - x_s(t) < 33\,m$ and $-8\,m/s^2 \leqslant a_{n,X}(t) \leqslant -2\,m/s^2$. Verification is required for the model outside this range. For enhanced performance, we recalibrate parameters C_0, C_1 and C_2 using two datasets.

A.2. Perceived Probabilistic Driving Risk Field Model (PPDRF)

Perceived Probabilistic Driving Risk Field Model (PPDRF) enhances the Probabilistic Driving Risk Field Model (PDRF) (Mullakkal-Babu et al., 2020) by accounting for diverse traffic scenarios and driver individuality. The model is inspired by artificial potential field used in driving automation (Wang et al., 2016; Li et al., 2020; Ni, 2013). PDRF estimates collision risk by considering potential risk from non-moving vehicles/objects and kinetic risk from other road users. The former accounts for collision energy and probability with stationary obstacles, while the latter involves spatial overlap with neighbouring vehicles using predicted positions and stochastic accelerations. In stable highway driving, the longitudinal and lateral accelerations of a neighbour follow a Gaussian distribution (Wagner et al., 2016; Ko et al., 2010). However, due to uncertainties and behavioural deviations, human drivers perceive risk differently, leading to a bias between objective and perceived risk. To address this, we introduce assumptions to extend PDRF into PPDRF for predicting perceived risk.

- The future acceleration in longitudinal and lateral directions of neighbouring vehicles follows independent Gaussian distributions with the current acceleration as the mean value, remaining constant over the prediction horizon;
- The subject vehicle maintains the current acceleration over the prediction horizon;

The two assumptions simplify road users' motion.

In PPDRF model, human drivers, at time t, perceive a total risk as a combination of kinetic risk and potential risk as follows

$$R_{PPDRF}(t) = R_{n,s}(t) + R_{o,s}(t) \tag{A.3}$$

The kinetic risk in PPDRF concerning moving neighbouring vehicles is given by

$$R_{n,s}(t) = 0.5 M_s \beta^2 \left|\Delta v_{s,n}(t+\tau)\right|^2 \cdot \tilde{p}(n, s \mid t) \tag{A.4}$$

where $R_{n,s}(t)$ is the kinetic collision risk between the subject vehicle s and a neighbouring vehicle n in Joules at time t. $\beta = \frac{M_n}{M_s + M_n}$ denotes the mass ratio. M_s and M_n are the mass of the subject vehicle and the neighbouring vehicle. $\Delta v_{s,n}(t+\tau)$ is the relative velocity between the subject vehicle and the neighbouring vehicle at time $t + \tau$. $\tilde{p}(n, s \mid t)$ is the collision probability to the neighbouring vehicle estimated by drivers ranging on [0, 1].

The collision probability $\tilde{p}(n, s \mid t)$ to the neighbouring vehicle estimated by human drivers is constructed as Eq. (A.5).

$$\tilde{p}(n, s \mid t) = \mathcal{N}\left(\frac{\Delta x(t) - \Delta v_X(t)\tau}{0.5\tau^2} \mid \mu_X(t), \tilde{\sigma}_X\right) \cdot \mathcal{N}\left(\frac{\Delta y(t) - \Delta v_Y(t)\tau}{0.5\tau^2} \mid \mu_Y(t), \tilde{\sigma}_Y\right) \tag{A.5}$$

where $\mathcal{N}$ is the assumed Gaussian collision probability density function (Fig. A.13). $\mu_X(t)$ and $\mu_Y(t)$ represent the mean values for longitudinal and lateral acceleration distribution, while $\tilde{\sigma}X$ and $\tilde{\sigma}Y$ are the respective standard deviations. The relative spacing and velocities between the subject and neighbouring vehicles are denoted as $\Delta x(t)$, $\Delta y(t)$, $\Delta v_X(t)$, and $\Delta v_Y(t)$. PPDRF evaluates collision probability using multiple values of $\tau = 0.5\,s, 1\,s, 2\,s, 3\,s$, with the model employing all these values to maximise the computed collision probability. Using the constant acceleration assumption, the predicted position of the subject vehicle and stochastic positions of neighbouring vehicles are calculated over a prediction horizon. Spatial overlap and collision predictions are determined accordingly. The actual $\tilde{p}(n, s \mid t)$ is obtained through integration over the expected accelerations.

The potential risk posed to vehicle s by a static object o can be modelled as

$$R_{o,s}(t) = 0.5 k M \left(\Delta v_{s,o}(t)\right)^2 \cdot \max\left(e^{-|r_{s,o}|/D}, 0.001\right) \tag{A.6}$$

where $R_{o,s}(t)$ denotes the potential risk caused by the static object o; M denotes the mass of s; $|r_{s,o}| = \|\boldsymbol{p}_s - \boldsymbol{p}_n\|$ is the distance between the subject vehicle s and the non-moving object o; $V_{s,o}$ denotes the relative velocity; $0.5kM(V_{s,o})^2$ represents the expected

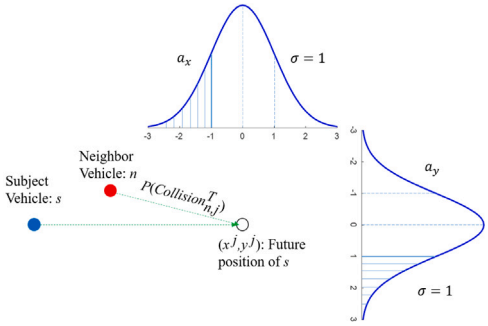

Fig. A.13. The acceleration distribution of the neighbouring vehicle and the relative spacing between the subject vehicle and the neighbouring vehicle.

crash energy scaled by the parameter k, with range [0–1], which is set to 1 in this study representing the neighbour is immovable; the term $e^{-|r_{s,o}|/D}$ is the collision probability ranging between [0–1], where D determines the steepness of descent of the potential field, varying among different drivers.

It is noteworthy that $R_{PPDRF}(t)$ represents a probabilistic energy value, and can attain up to 3×10^4 J under stable motorway driving conditions (Mullakkal-Babu et al., 2020).

A.3. Driving risk field model (DRF)

The DRF represents human drivers' risk perception as a 2D field, combining the probability (probability field) and consequence (severity field) of an event (Kolekar et al., 2020a), the product of which provides an estimation of driver's perceived risk. The DRF model was derived from a simulator experiment involving obstacle avoidance with 77 obstacles distributed on a 2D plane in front of the subject vehicle. During each drive, one obstacle was randomly chosen and suddenly appeared, after which participants needed to steer to avoid the obstacle and gave a non-negative number indicating required steering effort. Based on the position information of the obstacles, the maximum steering angle, and the subjective ratings, the DRF model was fitted to the data, and thereby it is essentially an empirical model. The DRF is based on the following assumptions:

- Perceived risk is the product of the probability of a hazardous event occurring estimated by drivers and the event severity;
- The perceived risk field widens as the longitudinal distance from the subject vehicle increases;
- The height of the perceived risk field decays as the lateral and longitudinal distance from the vehicle increases;

The DRF model quantifies overall perceived risk as

$$R_{DRF}(t) = \sum p(x(t), y(t)) \cdot sev(t) \tag{A.7}$$

where $p(x(t), y(t))$ is the probability of an event happening at position $(x(t), y(t))$; $sev(t)$ is the severity field of events. Specifically, in straight drive, the probability field can be simplified as

$$p(x(t), y(t)) = h \cdot \exp\left(\frac{-y(t)^2}{2\sigma^2}\right) \tag{A.8}$$

$$h = s \cdot \left(x(t) - v_{s,X}(t) \cdot t_{la}\right)^2 \tag{A.9}$$

$$\sigma = m \cdot x(t) + c \tag{A.10}$$

where the subject vehicle is at the origin $(0, 0)$ with h and σ representing the height and the width of the Gaussian at longitudinal position $x(t)$; s defines the steepness of the height parabola; t_{la} is the human driver's preview time (s); m defines the widening rate of the 2D probability field; c is the quarter width of the subject vehicle (m). $v_{s,X}(t)$ is the subject vehicle's velocity (m/s). The lateral cross-section of the 2D probability field is a Gaussian. Note that the height of the Gaussian h and the width σ are separately modelled as a parabola and linear function of longitudinal distance x in front of the subject vehicle.

The severity field of the events in this study can be defined as

$$sev(t) = \begin{cases} C_{sev}, & (x(t), y(t)) \in A^O, \\ 0, & (x(t), y(t)) \notin A^O. \end{cases} \tag{A.11}$$

where C_{sev} is the severity value that is set empirically and A^O represents a neighbouring vehicle's spatial area.

Appendix B. PCAD time history output

This Appendix presents the PCAD time history outputs in Dataset Merging (Fig. B.14) and Dataset Obstacle Avoidance (Fig. B.15).

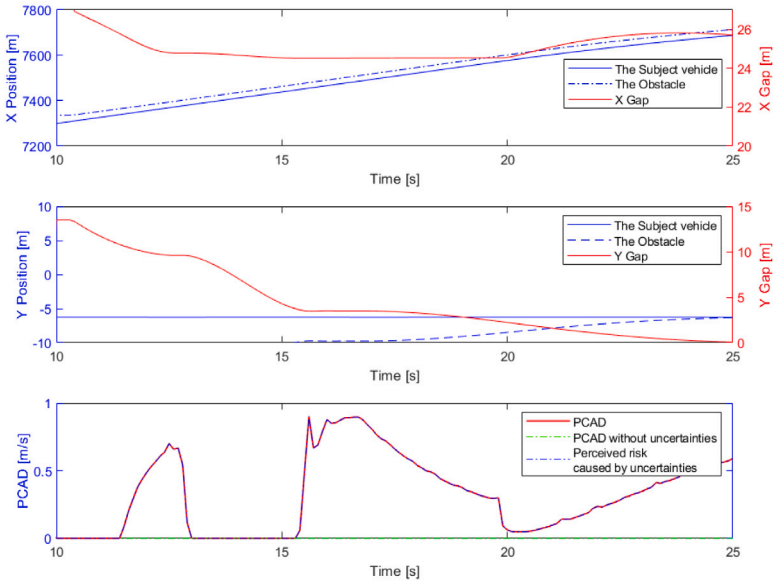

(a) Merging gap is 25 m and the deceleration of the merging vehicle is $-2\,\mathrm{m/s^2}$

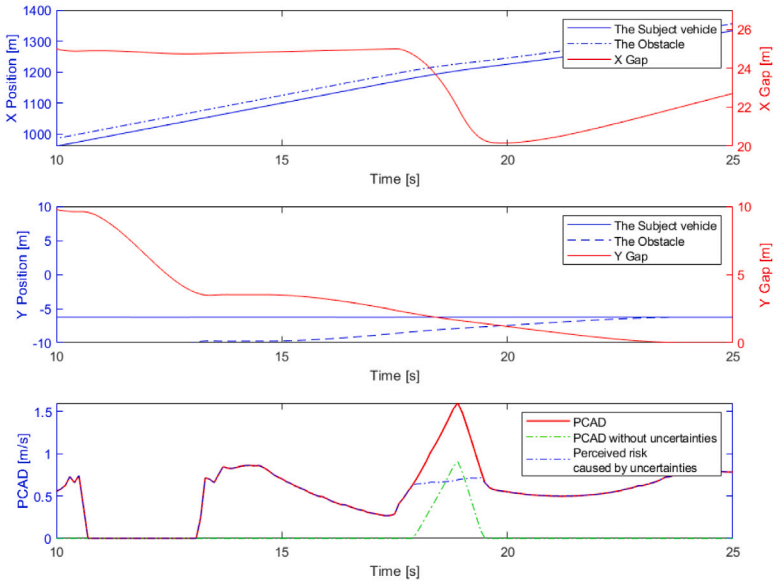

(b) Merging gap is 25 m and the deceleration of the merging vehicle is $-8\,\mathrm{m/s^2}$

Fig. B.14. PCAD historical output in merging and hard braking events.

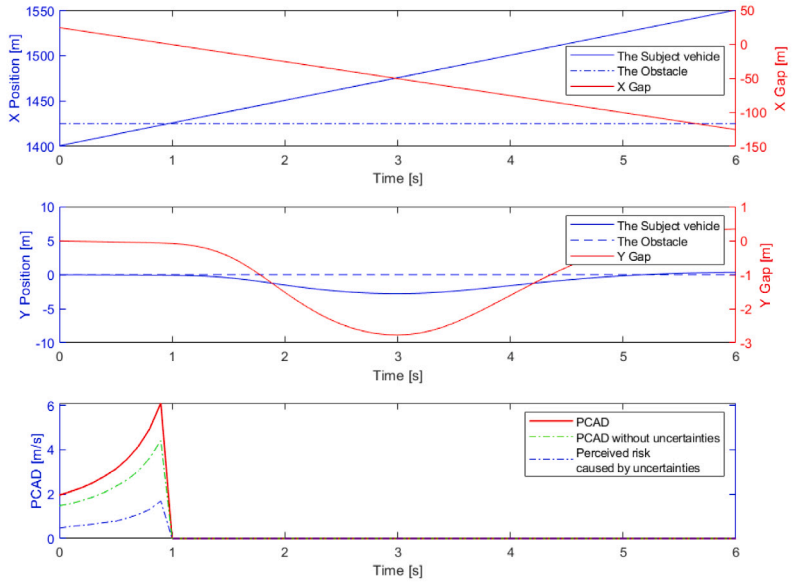

(a) The obstacle position is (25, 0), which means the obstacle is 25 m in front and the lateral offset is 0.

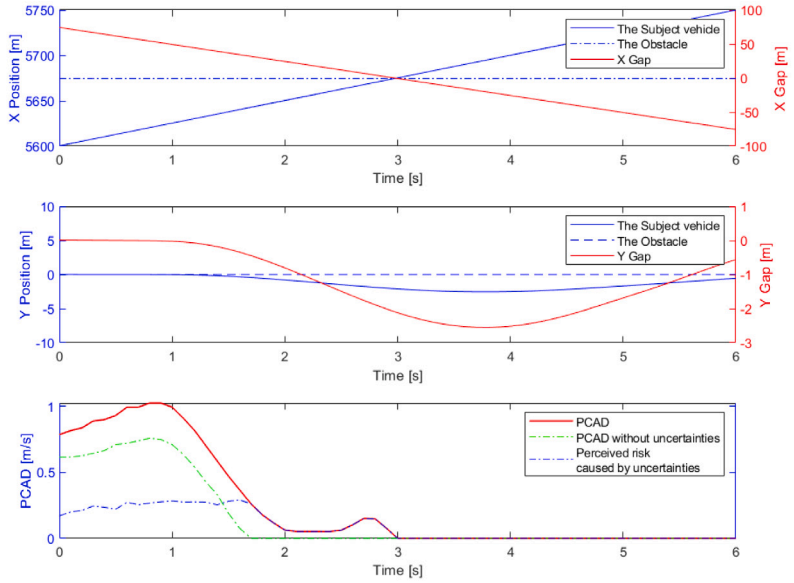

(b) The obstacle position is (75, 0), which means the obstacle is 75 m in front and the lateral offset is 0.

Fig. B.15. PCAD historical output in obstacle avoidance events.

Table C.6
Model performance indicators for the cross-validation.

Dataset	Performance indicators	PCAD	RPR	PPDRF	DRF
Dataset Merging (with parameters calibrated with Dataset Obstacle Avoidance)	$RMSE_{event}$	2.37	7.72	4.86	5.14
	$RMSE_{peak}$	3.73	8.29	5.14	5.79
	Adjusted R-Square	0.79	0.88	0.20	0.00
	Detection rate	1.00	1.00	1.00	1.00
	Computational cost (ms)	3.25	2.09×10^{-4}	1.03×10^{-2}	1.01
Dataset Obstacle Avoidance (with parameters calibrated with Dataset Merging)	$RMSE_{event}$	2.28	3.20	3.48	3.19
	$RMSE_{peak}$	2.73	3.84	3.93	3.87
	Adjusted R-Square	0.90	0.38	0.11	0.42
	Detection rate	1.00	0.09	1.00	1.00
	Computational cost (ms)	5.58	1.98×10^{-4}	7.28	1.82

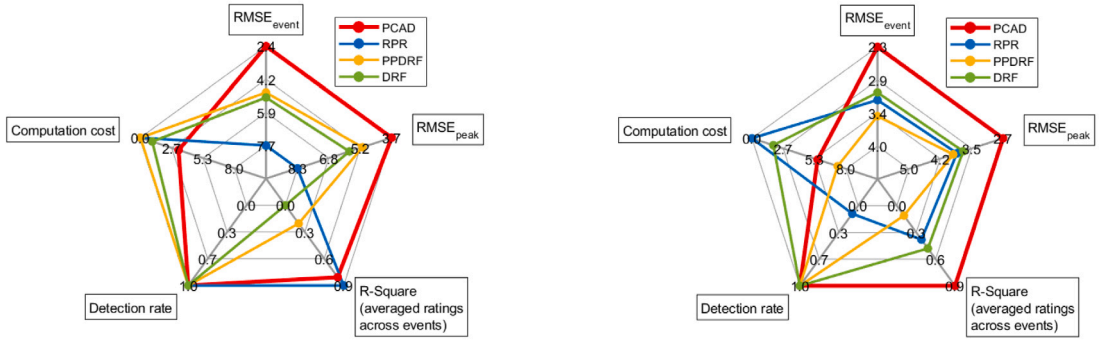

(a) Performances in Dataset Merging (with parameters calibrated with Dataset Obstacle Avoidance)

(b) Performances in Dataset Obstacle Avoidance (with parameters calibrated with Dataset Merging)

Fig. C.16. Radar chart of model performance indicators for the cross-validation.

Appendix C. Cross validation

This Appendix presents the model performance in cross-validation between the two datasets. See Table C.6, Figs. C.16–C.18.

Appendix D. Explanation of the uncertain velocity direction

In this Appendix, we explain why the line connecting the subject vehicle and the neighbouring vehicle is selected as the direction of the uncertain velocity.

With the uncertain velocity and the perceived velocity derived from acceleration, Eqs. (3) and (6) are changed to

$$\begin{aligned}\dot{\theta}'_{sj_1,nj_2} &= \frac{\left(\boldsymbol{p}_{sj_1}-\boldsymbol{p}_{nj_2}\right)\times\left(\boldsymbol{v}'_{sj_1}-\boldsymbol{v}'_{nj_2}\right)}{\left\|\boldsymbol{p}_{sj_1}-\boldsymbol{p}_{nj_2}\right\|^2}\\ &= \frac{\left(\boldsymbol{p}_{sj_1}-\boldsymbol{p}_{nj_2}\right)\times\left[\left(\boldsymbol{v}_{sj_1}+\Delta\boldsymbol{v}_{s,a}+\Delta\boldsymbol{v}_{s,u}\right)-\left(\boldsymbol{v}_{nj_2}+\Delta\boldsymbol{v}_{n,a}+\Delta\boldsymbol{v}_{n,u}\right)\right]}{\left\|\boldsymbol{p}_{sj_1}-\boldsymbol{p}_{nj_2}\right\|^2}\\ &= \dot{\theta}_{sj_1,nj_2}+\Delta\dot{\theta}_{sj_1,nj_2,a}+\Delta\dot{\theta}_{sj_1,nj_2,u},\quad j_1,j_2\in\{l,r\}\end{aligned} \tag{D.1}$$

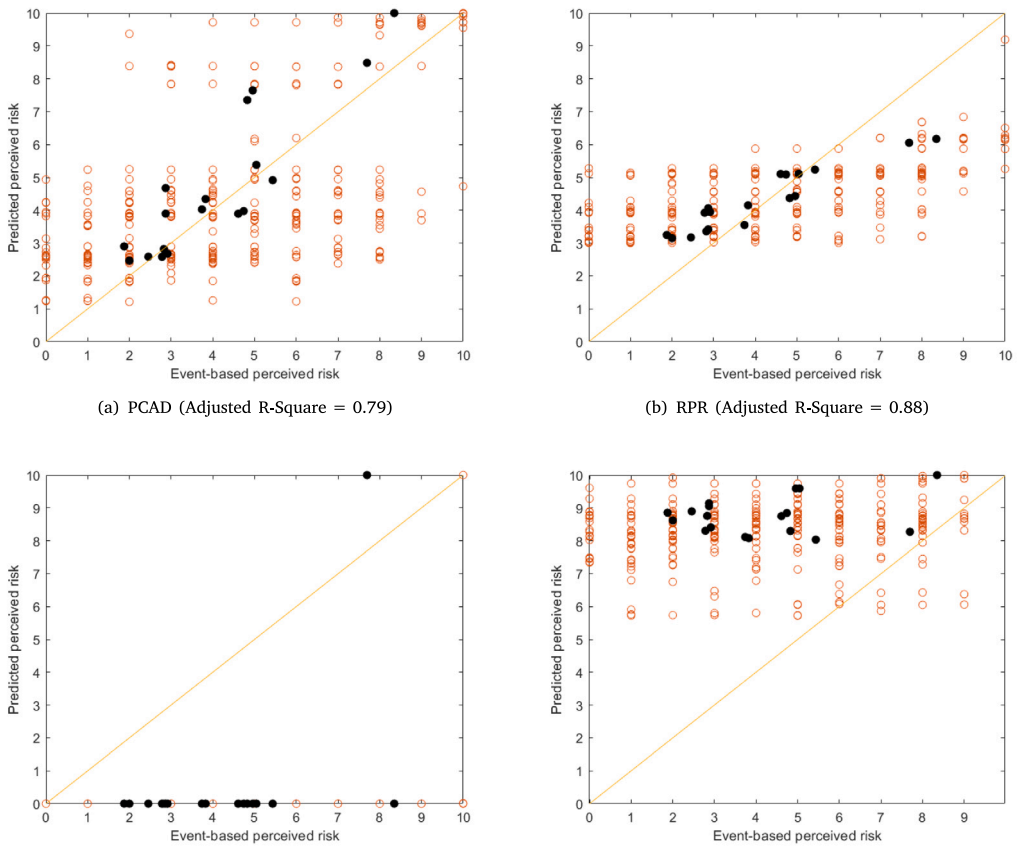

(a) PCAD (Adjusted R-Square = 0.79)

(b) RPR (Adjusted R-Square = 0.88)

(c) PPDRF (Adjusted R-Square = 0.20)

(d) DRF (Adjusted R-Square = 0.00)

Fig. C.17. Validation results in Dataset Merging with model parameters calibrated based on Dataset Obstacle Avoidance. '○' indicates raw event-based perceived risk and '●' indicates the averaged event-based perceived risk across the same event type.

and

$$\begin{aligned}\dot{d}'_{s,n} &= \frac{1}{d_{s,n}}(\boldsymbol{p}_s - \boldsymbol{p}_n)^T\left(\boldsymbol{v}'_s - \boldsymbol{v}'_n\right)\\ &= \frac{1}{d_{s,n}}(\boldsymbol{p}_s - \boldsymbol{p}_n)^T\left[(\boldsymbol{v}_s + \Delta\boldsymbol{v}_{s,a} + \Delta\boldsymbol{v}_{s,u}) - (\boldsymbol{v}_n + \Delta\boldsymbol{v}_{n,a} + \Delta\boldsymbol{v}_{n,u})\right]\\ &= \dot{d}_{s,n} + \dot{d}_{n,a} + \dot{d}_{s,n,u}\end{aligned} \tag{D.2}$$

where $\boldsymbol{v}'_s = \boldsymbol{v}_s + \Delta\boldsymbol{v}_{s,a} + \Delta\boldsymbol{v}_{s,u}$ and $\boldsymbol{v}'_n = \boldsymbol{v}_n + \Delta\boldsymbol{v}_{n,a} + \Delta\boldsymbol{v}_{n,u}$ are the perceived velocity with the uncertain velocity $\Delta\boldsymbol{v}_{s,u}$ and $\Delta\boldsymbol{v}_{n,u}$ for the subject vehicle and the neighbouring vehicle respectively.

In order to make the situation more dangerous, the uncertain velocity has to create a situation that is opposite to Eq. (9) namely

$$\min\dot{\boldsymbol{\theta}}_{si,nj,u}\cdot\max\dot{\boldsymbol{\theta}}_{si,nj,u} \leqslant 0\ (i,j\in\{l,r\},)\text{ and }\dot{d}_{s,n,u} < 0, \tag{D.3}$$

where all relative bearing rate and the distance changing rate are only caused by the uncertain velocity.

Comparing with Eq. (9), the optimal direction for the uncertain velocity based on Eq. (D.2) to create a negative distance changing rate should be

$$\begin{aligned}\begin{bmatrix}\frac{\partial\dot{d}_{s,n,u}}{\partial v_{s,X,u}}\\ \frac{\partial\dot{d}_{s,n,u}}{\partial v_{s,Y,u}}\end{bmatrix} &= \begin{bmatrix}\frac{\partial\dot{d}'_{s,n}}{\partial v_{s,X,u}}\\ \frac{\partial\dot{d}'_{s,n}}{\partial v_{s,Y,u}}\end{bmatrix} = \frac{1}{d_{s,n}}\begin{bmatrix}\Delta\boldsymbol{p}_X\\ \Delta\boldsymbol{p}_Y\end{bmatrix} = \frac{\boldsymbol{p}_s - \boldsymbol{p}_n}{\|\boldsymbol{p}_s - \boldsymbol{p}_n\|}\\ \begin{bmatrix}\frac{\partial\dot{d}_{s,n,u}}{\partial v_{n,X,u}}\\ \frac{\partial\dot{d}_{s,n,u}}{\partial v_{n,Y,u}}\end{bmatrix} &= \begin{bmatrix}\frac{\partial\dot{d}'_{s,n}}{\partial v_{n,X,u}}\\ \frac{\partial\dot{d}'_{s,n}}{\partial v_{n,Y,u}}\end{bmatrix} = \frac{1}{d_{s,n}}\begin{bmatrix}-\Delta\boldsymbol{p}_X\\ -\Delta\boldsymbol{p}_Y\end{bmatrix} = -\frac{\boldsymbol{p}_s - \boldsymbol{p}_n}{\|\boldsymbol{p}_s - \boldsymbol{p}_n\|}\end{aligned} \tag{D.4}$$

where $\Delta\boldsymbol{p}_X = \boldsymbol{p}_{s,X} - \boldsymbol{p}_{n,X}$, $\Delta\boldsymbol{p}_Y = \boldsymbol{p}_{s,Y} - \boldsymbol{p}_{n,Y}$.

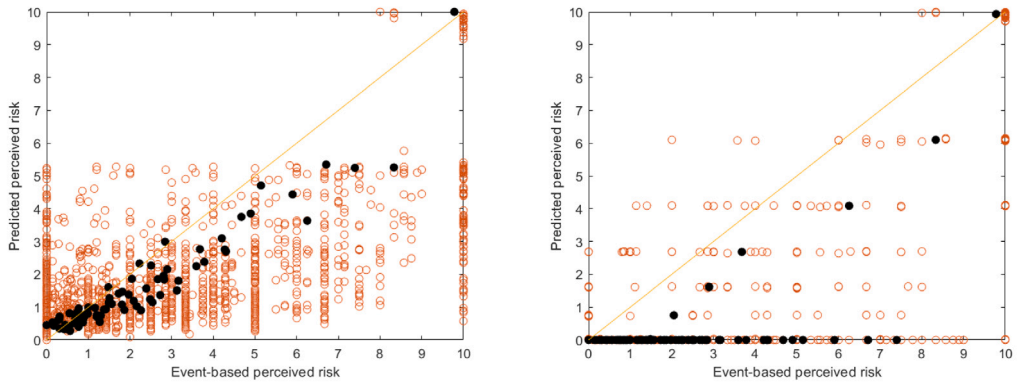

(a) PCAD (Adjusted R-Square = 0.90)

(b) RPR (Adjusted R-Square = 0.38)

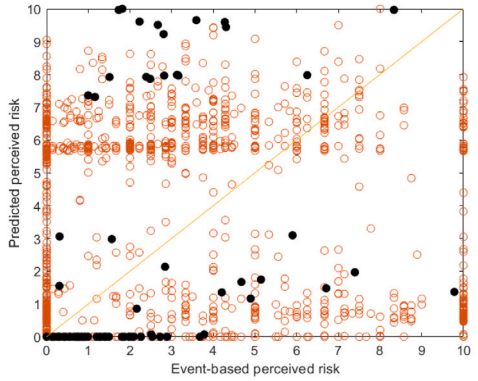

(c) PPDRF (Adjusted R-Square = 0.11)

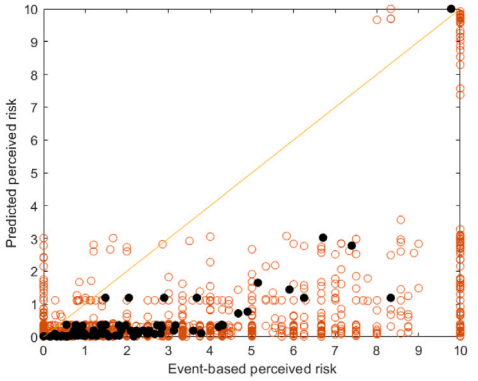

(d) DRF (Adjusted R-Square = 0.48)

Fig. C.18. Validation results in Dataset Obstacle Avoidance with model parameters calibrated based on Dataset Merging. '○' indicates raw event-based perceived risk and '●' indicates the averaged event-based perceived risk across the same event type.

Eq. (D.4) means that the distance direction is the optimal for the uncertain velocity of the subject vehicle and the neighbouring vehicle to create a negative distance changing rate in Eq. (D.3).

Simultaneously, the uncertain velocity should not cause extra relative bearing rate which makes the situation less dangerous. In other words, the uncertain velocity should follow the normal direction of the relative bearing rate gradient. Hence, the direction should be

$$\begin{aligned}\left[\begin{array}{c}\frac{\partial\theta_{s,n,u}}{\partial v_{s,X,u}}\\ \frac{\partial\theta_{s,n,u}}{\partial v_{s,Y,u}}\end{array}\right]\Bigg|_{\perp}=\left[\begin{array}{c}\frac{\partial\theta'_{s,n}}{\partial v_{s,X,u}}\\ \frac{\partial\theta'_{s,n}}{\partial v_{s,Y,u}}\end{array}\right]\Bigg|_{\perp}=\frac{1}{d_{s,n}^2}\left[\begin{array}{c}\Delta p_Y\\ -\Delta p_X\end{array}\right]\Bigg|_{\perp}=\frac{\boldsymbol{p}_s-\boldsymbol{p}_n}{\|\boldsymbol{p}_s-\boldsymbol{p}_n\|^2}\\ \left[\begin{array}{c}\frac{\partial\dot{\theta}'_{s,n}}{\partial v_{n,X,u}}\\ \frac{\partial\dot{\theta}'_{s,n}}{\partial v_{n,Y,u}}\end{array}\right]\Bigg|_{\perp}=\frac{1}{d_{s,n}^2}\left[\begin{array}{c}-\Delta p_Y\\ \Delta p_X\end{array}\right]\Bigg|_{\perp}=-\frac{\boldsymbol{p}_s-\boldsymbol{p}_n}{\|\boldsymbol{p}_s-\boldsymbol{p}_n\|^2}\end{aligned}\tag{D.5}$$

which are exactly the directions shown in Eq. (D.4). That means the distance direction is the optimal direction for the uncertain velocity to create a negative distance changing rate and in the meantime not to cause less perceived risk.

Appendix E. Supplementary data

Supplementary material related to this article can be found online at https://doi.org/10.1016/j.trc.2024.104751. A video representing the dynamics of the proposed model PCAD in a traffic event can be found via this link https://doi.org/10.4121/3ad2db22-ea82-4436-8df5-ebbbdb4aeec6.

References

Aarts, L., Van Schagen, I., 2006. Driving speed and the risk of road crashes: A review. Accid. Anal. Prev. 38 (2), 215–224.

Blaauw, G.J., 1982. Driving experience and task demands in simulator and instrumented car: a validation study. Hum. Factors 24 (4), 473–486.
Crashdashes, 2023. How many people in comments could do better. https://www.instagram.com/reel/CsKIpjSr78Z/?utm_source=ig_web_copy_link.
Ding, J., Wang, J., Liu, C., Lu, M., Li, K., 2014. A Driver steering behavior model based on lane-keeping characteristics analysis. In: 2014 17th IEEE International Conference on Intelligent Transportation Systems, ITSC 2014. IEEE, pp. 623–628.
Duan, J., Li, Z., Salvendy, G., 2013. Risk illusions in car following: Is a smaller headway always perceived as more dangerous? Saf. Sci. 53, 25–33.
Eboli, L., Mazzulla, G., Pungillo, G., 2017. How to define the accident risk level of car drivers by combining objective and subjective measures of driving style. Transp. Res. F 49, 29–38.
Finch, D., Kompfner, P., Lockwood, C., Maycock, G., 1994. Speed, speed limits and crashes. Crowthorne, berkshire. Transport Research Laboratory TRL, Project Report PR, 58.
Fuller, R., 1984. A conceptualization of driving behaviour as threat avoidance. Ergonomics 27 (11), 1139–1155.
Fuller, R., 1999. The Task-Capability Interface model of the driving process.
Fuller, R., 2011. Driver control theory: From task difficulty homeostasis to risk allostasis. In: Handbook of Traffic Psychology. Elsevier, pp. 13–26.
Griffin, W., Haworth, N., Twisk, D., 2020. Patterns in perceived crash risk among male and female drivers with and without substantial cycling experience. Transp. Res. F 69, 1–12.
He, X., Stapel, J., Wang, M., Happee, R., 2022. Modelling perceived risk and trust in driving automation reacting to merging and braking vehicles. Transp. Res. F 86 (February), 178–195.
Herman, R., Montroll, E.W., Potts, R.B., Rothery, R.W., 1959. Traffic dynamics: studies in car following. Oper. Res. 6 (2), 165–184.
Hu, C., Wang, J., 2021. Trust-based and individualizable adaptive cruise control using control barrier function approach with prescribed performance. IEEE Trans. Intell. Transp. Syst. 1–11.
Jansson, J., 2005. Collision Avoidance Theory: With Application to Automotive Collision Mitigation (Ph.D. thesis). Linköping University Electronic Press.
Jazar, R.N., 2008. Vehicle Dynamics. vol. 1, Springer.
Jouhri, A., Sharkawy, A., Paksoy, H., Youssif, O., He, X., Kim, S., Happee, R., 2023. The influence of a colour themed HMI on trust and take-over performance in automated vehicles. Front. Psychol. 14.
Kiefer, R.J., Leblanc, D.J., Flannagan, C.A., 2005. Developing an inverse time-to-collision crash alert timing approach based on drivers' last-second braking and steering judgments. Accid. Anal. Prev. 37 (2), 295–303.
Kim, S., He, X., van Egmond, R., Happee, R., 2024. Designing user interfaces for partially automated Vehicles: Effects of information and modality on trust and acceptance. Transportation research part F: traffic psychology and behaviour 103, 404–419.
Ko, J., Guensler, R., Hunter, M., 2010. Analysis of effects of driver/vehicle characteristics on acceleration noise using GPS-equipped vehicles. Transp. Res. F 13 (1), 21–31.
Kochi, F., Saito, Y., Uchida, N., Itoh, M., 2023. Task difficulty, risk feeling, and safety margin in the determination of driver behavior to prepare for traffic conflicts. Accid. Anal. Prev. 192, 107284.
Kolekar, S., De Winter, J., Abbink, D., 2020a. Human-like driving behaviour emerges from a risk-based driver model. Nature Commun. (September), 1–19.
Kolekar, S., de Winter, J., Abbink, D., 2020b. Which parts of the road guide obstacle avoidance? Quantifying the driver's risk field. Appl. Ergon. 89 (July), 103196.
Kondoh, T., Furuyama, N., Hirose, T., Sawada, T., 2014. Direct evidence of the inverse of TTC hypothesis for driver's perception in car-closing situations. Int. J. Autom. Eng. 5 (4), 121–128.
Kondoh, T., Yamamura, T., Kitazaki, S., Kuge, N., Boer, E.R., 2008. Identification of visual cues and quantification of drivers' perception of proximity risk to the lead vehicle in car-following situations. J. Mech. Syst. Transp. Logist. 1 (2), 170–180.
Lee, D., 1976. A theory of visual control of braking based on information about time-to- collision. Perception 5, 437–459.
Li, L., Gan, J., Yi, Z., Qu, X., Ran, B., 2020. Risk perception and the warning strategy based on safety potential field theory. Accid. Anal. Prev. 148 (December).
McKenna, F.P., 1982. The human factor in driving accidents an overview of approaches and problems. Ergonomics 25 (10), 867–877.
Mullakkal-Babu, F.A., Wang, M., He, X., van Arem, B., Happee, R., 2020. Probabilistic field approach for motorway driving risk assessment. Transp. Res. C 118 (July), 102716.
Näätänen, R., Summala, H., 1976. Road-user behaviour and traffic accidents. Publication of: North-Holland Publishing Company.
Nadimi, N., Behbahani, H., Shahbazi, H.R., 2016. Calibration and validation of a new time-based surrogate safety measure using fuzzy inference system. J. Traffic Transp. Eng. (Engl. Ed.) 3 (1), 51–58.
Ni, D., 2013. A unified perspective on traffic flow theory part I : The field theory. Appl. Math. Sci. 7 (39), 1929–1946.
Peng, C., Horn, S., Madigan, R., Marberger, C., Lee, J.D., Krems, J., Beggiato, M., Romano, R., Wei, C., Wooldridge, E., et al., 2024. Conceptualising user comfort in automated driving: Findings from an expert group workshop. Transp. Res. Interdiscip. Perspect. 24, 101070.
Ping, P., Sheng, Y., Qin, W., Miyajima, C., Takeda, K., 2018. Modeling driver risk perception on city roads using deep learning. IEEE Access 6, 68850–68866.
Rundmo, T., Nordfjærn, T., 2017. Does risk perception really exist? Saf. Sci. 93, 230–240.
Sivak, M., 1996. The information that drivers use: is it indeed 90% visual? Perception 25 (9), 1081–1089.
Sultan, B., Brackstone, M., McDonald, M., 2004. Drivers' use of deceleration and acceleration information in car-following process. Transp. Res. Rec. 1883 (1), 31–39.
Summala, H., 1988. Risk control is not risk adjustment: The zero-risk theory of driver behaviour and its implications. Ergonomics 31 (4), 491–506.
Wagner, P., Nippold, R., Gabloner, S., Margreiter, M., 2016. Analyzing human driving data an approach motivated by data science methods. Chaos Solitons Fractals 90, 37–45.
Wang, J., Wu, J., Zheng, X., Ni, D., Li, K., 2016. Driving safety field theory modeling and its application in pre-collision warning system. Transp. Res. C 72, 306–324.
Ward, J.R., Agamennoni, G., Worrall, S., Bender, A., Nebot, E., 2015. Extending Time to Collision for probabilistic reasoning in general traffic scenarios. Transp. Res. C 51, 66–82.
World Health Organization, 2020. Road traffic injuries. Retrieved May 28, 2023, from https://www.who.int/health-topics/road-safety#tab=tab_1.
Xu, Z., Zhang, K., Min, H., Wang, Z., Zhao, X., Liu, P., 2018. What drives people to accept automated vehicles? Findings from a field experiment. Transp. Res. C 95 (February), 320–334.